

Recursive Gaussian Process State Space Model

Tengjie Zheng^{*} and Haipeng Chen[†] and Lin Cheng[‡] and Shengping Gong[§] and Xu Huang[¶]

School of Astronautics, Beihang University, Beijing, 102206, China

State Key Laboratory of High-Efficiency Reusable Aerospace Transportation Technology, Beijing, 102206, China

Learning dynamical models from data is not only fundamental but also holds great promise for advancing principle discovery, time-series prediction, and controller design. Among various approaches, Gaussian Process State-Space Models (GPSSMs) have recently gained significant attention due to their combination of flexibility and interpretability. However, for online learning, the field lacks an efficient method suitable for scenarios where prior information regarding data distribution and model function is limited. To address this issue, this paper proposes a recursive GPSSM method with adaptive capabilities for both operating domains and Gaussian process (GP) hyperparameters. Specifically, first-order linearization is first applied to derive a Bayesian update equation for the joint distribution between the system state and the GP model, enabling closed-form and domain-independent learning. Second, an online selection algorithm for inducing points is developed based on informative criteria to achieve lightweight learning. Third, to support online hyperparameter optimization, historical measurement information is recovered from the current filtering distribution. Comprehensive evaluations on both synthetic and real-world datasets demonstrate the superior accuracy, computational efficiency, and adaptability of the proposed method compared to state-of-the-art online GPSSM techniques.

Nomenclature

\mathcal{GP}	=	Gaussian process (GP)
$m_0(\cdot)$	=	prior mean function of the GP
$K_0(\cdot, \cdot; \theta)$	=	prior covariance function (or kernel) of the GP
θ	=	kernel hyperparameters, nondimensional unit
K_{ab}	=	kernel matrix indexed by function outputs or function inputs, nondimensional unit

^{*}Ph.D. Candidate, School of Astronautics, ZhengTengjie@buaa.edu.cn.

[†]Research Fellow, China Academy of Launch Vehicle Technology, Hitchenhp@163.com

[‡]**Corresponding Author**, Associate Professor, School of Astronautics, chenglin5580@buaa.edu.cn.

[§]Professor, School of Astronautics, gongsp@buaa.edu.cn.

[¶]Associate Professor, School of Astronautics, xunudt@126.com.

k_{ab}	= $K_{ab}K_{bb}^{-1}$, nondimensional unit
Σ_p	= process noise covariance, nondimensional unit
Σ_m	= measurement noise covariance, nondimensional unit
\mathbf{x}_t	= system state at time t , nondimensional unit
\mathbf{y}_t	= measurement at time t , nondimensional unit
$\mathbf{F}(\cdot)$	= known transition function structure
$f(\cdot)$	= unknown component of the transition function $\mathbf{F}(\cdot)$
$\mathbf{g}(\cdot)$	= measurement function
f	= all function values of $f(\cdot)$, nondimensional unit
\mathbf{u}	= inducing point set, nondimensional unit
$f_{\neq u}$	= function values of $f(\cdot)$ excluding the inducing points \mathbf{u} , nondimensional unit
$p(\cdot)$	= exact probability density function
$q(\cdot)$	= approximate probability density function
μ_t	= mean of the system state \mathbf{x} at time t , nondimensional unit
\mathbf{P}_t	= covariance of the system state \mathbf{x} at time t , nondimensional unit
\mathbf{m}_u	= mean of the inducing points \mathbf{u} , nondimensional unit
V_{xu}	= cross-covariance between the system state \mathbf{x} and the inducing points \mathbf{u} , nondimensional unit
S_{uu}	= auto-covariance of the inducing points \mathbf{u} , nondimensional unit
f_t	= function value $f(\mu_t)$, nondimensional unit
m_{f_t}	= mean of the function value f_t , nondimensional unit
\mathbf{F}_t	= predicted mean of the state transition function, i.e., $\mathbf{F}_t = \mathbf{F}(\mu_t, m_{f_t})$, nondimensional unit
\mathbf{A}_f	= transition Jacobian with respect to the function value f_t , nondimensional unit
\mathbf{A}_x	= transition Jacobian with respect to the state \mathbf{x} , nondimensional unit
\mathbf{C}_x	= measurement Jacobian with respect to the state \mathbf{x} , nondimensional unit
$\bar{\mathbf{u}}$	= augmented inducing point set, i.e., $\bar{\mathbf{u}} = [\mathbf{u}^T, f_t^T]^T$, nondimensional unit
\mathbf{X}_t	= augmented state at time t , i.e., $\mathbf{X}_t = [\mathbf{x}_t^T, \mathbf{u}^T]^T$, nondimensional unit
ξ_t	= mean of the augmented state \mathbf{X}_t , nondimensional unit
Σ_t	= covariance of the augmented state \mathbf{X}_t , nondimensional unit
$\bar{\mathbf{X}}_t$	= augmented state with $\bar{\mathbf{u}}$, i.e., $\bar{\mathbf{X}}_t = [\mathbf{x}_t^T, \bar{\mathbf{u}}^T]^T$, nondimensional unit
$\bar{\xi}_t$	= mean of the augmented state $\bar{\mathbf{X}}_t$, nondimensional unit
$\bar{\Sigma}_t$	= covariance of the augmented state $\bar{\mathbf{X}}_t$, nondimensional unit
Φ	= transition Jacobian for the augmented state $\bar{\mathbf{X}}_t$, nondimensional unit

$\Sigma_{p,X}$	=	process noise covariance for the augmented state \bar{X}_t , nondimensional unit
H	=	measurement Jacobian for the augmented state \bar{X}_t , nondimensional unit
M	=	budget for inducing point set size, nondimensional unit
u_d	=	inducing point to be discarded, nondimensional unit
u_l	=	inducing points left after discarding, nondimensional unit
i_d	=	index of the inducing point to be discarded
s_d	=	score evaluating the importance of the inducing points, nondimensional unit
Q	=	inversion of the kernel matrix K_{uu}^{-1} , nondimensional unit
Ω	=	inversion of the joint covariance Σ_t^{-1} , nondimensional unit
Q_{dd}	=	the i_d -th diagonal element of the matrix Q , nondimensional unit
Q_{du}	=	the i_d -th row of the matrix Q , nondimensional unit
Ω_{dd}	=	the $(d_x + i_d)$ -th diagonal element of the matrix Ω , nondimensional unit
γ	=	novelty metric for inducing points, nondimensional unit
ε_{tol}	=	threshold for adding inducing points, nondimensional unit
Superscripts		
–	=	predicted distribution
*	=	optimal distribution
old	=	old GP hyperparameters
new	=	new GP hyperparameters

I. Introduction

STATE-space models (SSMs), also known as hidden Markov models (HMMs), describe the evolution and observation processes of latent states through a state transition model and a measurement model. By summarizing historical information into the latent state, SSMs provide a concise representation of system dynamics and are widely applied in fields such as aerospace engineering [1, 2], target tracking [3–5], and control systems [6–9]. Nevertheless, due to the complexity of real-world systems, establishing precise SSMs based on first principles is challenging. To achieve sufficiently accurate system models, extensive research has focused on data-driven SSM modeling [10–13].

In the past decade, a novel SSM learning method based on the Gaussian process (GP), a nonparametric modeling technique, has been explored [12, 14]. Mathematically, a GP is a probability distribution over functions, providing a flexible and probabilistic framework for modeling unknown functions. GPs not only yield predictions but also quantify uncertainty, making them widely used in machine learning [15] and system identification [16]. Over the past 30 years, many limitations of GPs, including cubic computational complexity, limited representational capacity, and challenges

with online learning, have been gradually overcome. For example, various sparse approximation techniques have been developed, such as inducing point methods [17, 18], spectrum approximations [19, 20] and Vecchia approximation [21]. Recent advances in scalable GPs [22, 23] have enabled GPs to handle datasets with millions of points. To improve representational power, deep GPs [24, 25] and ensemble GPs [26] have been developed by stacking multiple layers of GPs and mixing multiple GPs, respectively. Besides, online extensions like sparse online GPs [27], local GPs [28], and streaming sparse GPs [29] have equipped GPs with the ability to process streaming data. Therefore, GPs have gradually become a powerful tool for various applications.

Building on the aforementioned advances, GPs have been naturally developed for the modeling of dynamical systems. In the context of SSM learning, GPs can be employed to model the transition and measurement functions, resulting in what are known as Gaussian process state-space models (GPSSMs) [12]. By employing GPs, GPSSMs offer flexible learning for the dynamical system and provide prediction uncertainty, which is crucial for safety-critical applications [30]. To date, various GPSSM methods have been developed, including sample-based methods [31–34] and variational inference (VI)-based methods [35–39]. For example, the early variational GPSSM method proposed by Frigola et al. [32] combines variational Bayes and sequential Monte Carlo (SMC) to learn the GPSSM by iteratively updating the GP and state trajectory. Subsequently, the probabilistic recurrent state space model (PRSSM) [36] adopts the training approach of recurrent neural networks (RNNs) to optimize the variational posterior of the initial state and GP. In view of the limitation of the mean-field assumption in PRSSM, the variationally coupled dynamic trajectories (VCDT) [37] parameterize the coupling between the state and inducing points. Recently, the ensemble Kalman filter-aided variational inference (EnVI) [39] employs the ensemble Kalman filter (EnKF) to capture the coupling between state and GP, eliminating the need for the additional inference network required in previous methods. These methods have achieved significant progress in GPSSM learning, but most studies focus solely on offline scenarios. In engineering practice, many systems experience non-stationary changes (e.g., drone propeller performance varies with battery levels), and there is the possibility of operating in out-of-distribution settings. Therefore, this underscores the urgent need for online learning methods for GPSSMs, which is the focus of this paper.

Facilitating online learning for GPSSMs presents significant challenges. Beyond the usual constraints associated with online learning—such as minimizing memory usage, reducing computational complexity, and preventing catastrophic forgetting—GPSSMs pose additional, unique difficulties. These challenges are detailed as follows. **(1) Nonlinearity complicates inference.** In GPSSMs, the system state is included in the input to the GP model, introducing inherent nonlinearity. This nonlinearity is intractable, which prevents exact inference through analytic methods. **(2) Nonparametric nature of GP.** For standard Gaussian process regression (GPR), the training complexity scales cubically with the number of samples [15]. In an online context, as new data arrives continuously, the computational cost of GPs increases rapidly, rendering inference intractable. **(3) Coupling between the system state and the system model.** Since the state is implicitly measured in general, learning the system model requires inferring the system state. However, state

inference depends on the system model itself. As a result, there is a coupling between the state and the model, which increases the complexity of inference. Theoretically, since both are uncertain, they should be treated as latent variables and inferred simultaneously. **(4) Hyperparameter online optimization.** GPSSMs involve several hyperparameters, such as GP kernel parameters, which impact the learning accuracy. In online settings, hyperparameter optimization presents two main challenges. First, due to memory efficiency considerations, historical measurements are not retained in online scenarios, depriving hyperparameter optimization of explicit information sources. Secondly, since the GP prior depends on kernel hyperparameters, tuning these parameters requires corresponding adjustments to the posterior distribution. Hence, the online GPSSM problem is quite challenging, and as a result, relevant research remains limited.

Theoretically, implementing online GPSSMs involves Bayesian inference. Therefore, existing methods primarily rely on Bayesian filtering or online variational inference techniques, which can be classified into three categories:

- 1) Augmented Kalman Filter (AKF)-based method [40–42]. This approach can jointly infer the system state and the GP model online, and its implementation involves two steps: first, parameterizing the GP with a limited number of parameters using inducing-point approximation [40, 41], or spectrum approximation [42]; and second, augmenting the GP model parameters into the state space and inferring the augmented state using the extended Kalman filter (EKF). Through the AKF-based framework, this method achieves recursive learning and offers advantages in learning speed and stability. However, there is a key limitation: the parameterization of the GP requires prior knowledge of the operating domain, specifically the location of inducing points or the range of basis functions in spectrum approximation [42]. This drawback limits the approach’s ability to adapt to the flexible distribution of online data. In addition, there is no feasible method for hyperparameter optimization for this approach.
- 2) Particle Filter (PF)-based method [43–45]. This approach is based on the paradigm of the Rao-Blackwellized Particle Filter [46]. It is similar to the AKF-based method, with the key difference being the use of the particle filter (PF) for the inference process. Since PF is inefficient at handling high-dimensional states, GP parameters are not augmented into the state space. Instead, each particle is assigned a GP, which is recursively learned using the particle state. This method can theoretically achieve precise inference for arbitrary observational distributions, provided the number of particles is sufficient. However, despite the inherent issues with PF, such as high computational cost and particle degeneracy [47], it also requires prior knowledge of the operating domain.
- 3) Stochastic Variational Inference (SVI)-based method [32, 39, 48]. This approach extends the offline variational inference method of GPSSMs by utilizing stochastic optimization techniques. It aims to retain many of the benefits of offline GPSSMs, such as a flexible operating domain and hyperparameter optimization capabilities. However, stochastic optimization assumes that the data subsampling process is uniformly random, which is not the case in most online situations. As a result, the learning process is driven by instantaneous data, leading to slow learning and catastrophic forgetting.

In summary, the existing methods either lack the ability to tune the operating domains and hyperparameters, or they face issues with learning speed and convergence.

To overcome the aforementioned shortcomings, a recursive learning algorithm for GPSSMs is proposed in this paper, capable of online adaptation to the operating domain and GP hyperparameters. The main contributions can be summarized as follows: Firstly, to implement a domain-independent recursive learning algorithm for GPSSMs, a novel Bayesian update equation is derived without pre-parameterizing the GP. In the derivation process, only mild linearization approximations are applied to achieve a closed-form solution, offering advantages in learning speed and stability. Through continuously expanding the inducing-point set, this method can accommodate real-time data distributions. Secondly, to address the computational cost issue caused by the increasing number of inducing points, an selection algorithm is developed with both addition and removal operations. To minimize accuracy loss, an optimal discarding equation and selection metric for inducing points are derived based on informative criteria. Thirdly, to alleviate the burden of offline hyperparameter tuning, an online GP hyperparameter optimization method is proposed. In this method, an approximate observation likelihood model is extracted from the obtained posterior distribution. Utilizing this likelihood model as the information source, the GP hyperparameters are optimized, and the posterior distribution can be adjusted as the hyperparameters change. Fourthly, to ensure numerical stability, a stable implementation method based on Cholesky decomposition is developed. Additionally, the extension to multi-output GP is provided, which significantly enhances the practicality and flexibility. Finally, the effectiveness of the proposed method is validated through two synthetic simulations and a real-world dataset. The experimental results demonstrate the superior accuracy, computational efficiency, and adaptability of the proposed method compared to state-of-the-art online GPSSM techniques.

II. Problem Formulation

In this section, we first briefly provide the background of Gaussian processes (GPs) and then give a definition of Gaussian process state-space models (GPSSMs) and the associated online learning problem.

A. Gaussian Processes

Mathematically, a GP is a probability distribution over function space, which has been developed for regression tasks. For learning a single-output function $f(\cdot)$, one can first place a GP prior on it:

$$f(\mathbf{x}) \sim \mathcal{GP}(m_0(\mathbf{x}), K_0(\mathbf{x}, \mathbf{x}'; \boldsymbol{\theta})) \quad (1)$$

where $m_0(\cdot)$ denotes the prior mean function and $K_0(\cdot, \cdot)$ represents the prior covariance function (also known as kernel function), and $\boldsymbol{\theta}$ denotes the kernel hyperparameters. As a common setting, we assume zero-mean GP prior, namely,

$m_0(\cdot) \equiv 0$. Then, given noise-free function values $\mathbf{f}_\mathcal{X} = \{f(\mathbf{x}_i)\}_{i=1}^{n_\mathcal{X}}$ at inputs $\mathcal{X} = \{\mathbf{x}_i\}_{i=1}^{n_\mathcal{X}}$, the posterior distribution for test function values $\mathbf{f}_* = \{f(\mathbf{x}_i^*)\}_{i=1}^{n_{\mathcal{X}^*}}$ at inputs $\mathcal{X}^* = \{\mathbf{x}_i^*\}_{i=1}^{n_{\mathcal{X}^*}}$ is [15]:

$$p(\mathbf{f}_*|\mathbf{f}_\mathcal{X}) = \mathcal{N}(\mathbf{K}_{*\mathcal{X}}\mathbf{K}_{\mathcal{X}\mathcal{X}}^{-1}\mathbf{f}_\mathcal{X}, \mathbf{K}_{**} - \mathbf{K}_{*\mathcal{X}}\mathbf{K}_{\mathcal{X}\mathcal{X}}^{-1}\mathbf{K}_{\mathcal{X}*}) \quad (2)$$

Here, we use shorthand notation for the kernel matrix, e.g., \mathbf{K}_{**} denotes the auto-covariance of \mathbf{f}_* , and $\mathbf{K}_{*\mathcal{X}}$ the cross-covariance between \mathbf{f}_* and $\mathbf{f}_\mathcal{X}$. This notation convention is consistently used throughout the entire text. The above discussion is based on single-output GPs, but indeed GPs can be utilized to learn multi-output functions by employing an associated kernel. However, for simplicity and clarity, the proposed method is elaborated first based on the single-output GP, and the extension to the multi-output case is discussed in Section V.A. Hence, in the following, the function to learn will be denoted as $f(\cdot)$ without boldface.

B. Online Gaussian Process State Space Models

In this paper, we consider the following discrete-time state-space model (SSM):

$$\begin{aligned} \mathbf{x}_{t+1} &= \mathbf{F}(\mathbf{x}_t, f(\mathbf{x}_t)) + \boldsymbol{\omega}_p, & \boldsymbol{\omega}_p &\sim \mathcal{N}(\mathbf{0}, \boldsymbol{\Sigma}_p) \\ \mathbf{y}_t &= \mathbf{g}(\mathbf{x}_t) + \boldsymbol{\omega}_m, & \boldsymbol{\omega}_m &\sim \mathcal{N}(\mathbf{0}, \boldsymbol{\Sigma}_m) \end{aligned} \quad (3)$$

where the vector $\mathbf{x} \in \mathbb{R}^{d_x}$ and $\mathbf{y} \in \mathbb{R}^{d_y}$ respectively denote the system state and measurement. The vectors $\boldsymbol{\omega}_p$ and $\boldsymbol{\omega}_m$ represent the process and measurement noise, with covariances $\boldsymbol{\Sigma}_p$ and $\boldsymbol{\Sigma}_m$, respectively. Additionally, the function $\mathbf{F} : \mathbb{R}^{d_x} \rightarrow \mathbb{R}^{d_x}$ denotes a known function structure for the transition model*, which contains an unknown component, represented as the function $f : \mathbb{R}^{d_x} \rightarrow \mathbb{R}$. To ensure identifiability, the measurement model $\mathbf{g} : \mathbb{R}^{d_x} \rightarrow \mathbb{R}^{d_y}$ is assumed to be known†.

To learn the unknown SSMs, GPSSMs place GP priors on the unknown function $f(\cdot)$, resulting in the following model [12]:

*This structure of $\mathbf{F}(\cdot)$ can represent various models of interest, such as when only some dimensions of the transition model are unknown, or a discretized continuous-time transition model $\mathbf{F}(\mathbf{x}_t, f(\mathbf{x}_t)) = \mathbf{x}_t + f(\mathbf{x}_t)\Delta t$, where Δt is the time step and the unknown component is the time-derivative model $\dot{\mathbf{x}} = f(\mathbf{x})$. Through using a varying time step Δt , the latter can be used for irregular measurement scenarios commonly occurring in biochemical sciences.

†Even if the measurement model is unknown in practice, we can augment the measurement \mathbf{y} into the state space and transform the problem into one with a known measurement model [12].

$$\mathbf{x}_0 \sim p(\mathbf{x}_0) \quad (4a)$$

$$f(\cdot) \sim \mathcal{GP}(m_0(\cdot), K_0(\cdot, \cdot; \theta)) \quad (4b)$$

$$\mathbf{x}_{t+1} | \mathbf{x}_t, \mathbf{f} \sim \mathcal{N}(\mathbf{x}_t | \mathbf{F}(\mathbf{x}_t, \mathbf{f}(\mathbf{x}_t)), \Sigma_p) \quad (4c)$$

$$\mathbf{y}_t | \mathbf{x}_t \sim \mathcal{N}(\mathbf{y}_t | \mathbf{g}(\mathbf{x}_t), \Sigma_m) \quad (4d)$$

where $p(\mathbf{x}_0)$ denotes a prior Gaussian distribution for the initial state \mathbf{x}_0 , and we use the notation \mathbf{f} to denote all function values of the function $f(\cdot)$. For conciseness, we omit the system input from the transition and measurement models, which can be easily incorporated by augmenting it into the input of these models and the function $f(\cdot)$.

In the online setting, measurements \mathbf{y} arrive sequentially, and we assume that historical measurements are not retained for computational and storage reasons. Given this streaming data setting, the inference task of online GPSSMs is to sequentially approximate the filtering distribution $p(\mathbf{x}_t, \mathbf{f} | \mathbf{y}_{1:t})$, using the previous result $p(\mathbf{x}_{t-1}, \mathbf{f} | \mathbf{y}_{1:t-1})$ and the current measurement \mathbf{y}_t . As illustrated in the introduction, several challenges exist in this task, including the nonlinearity and coupling involved, as well as the nonparametric nature of GPs and the hyperparameter optimization problem. To address these difficulties, a novel online GPSSM approach will be developed in the next two sections, with the ability to adapt to both operating domains and hyperparameters.

III. Bayesian Update Equation for Online GPSSMs

This section derives a Bayesian update equation for online GPSSMs with minimal approximations to achieve recursive learning in an arbitrarily operating domain.

A. Two-Step Inference

The online inference of GPSSMs is essentially a filtering problem for the hidden Markov model; therefore, most methods are based on filtering techniques, such as the extended Kalman filter (EKF) and particle filter (PF). Considering that the PF will exacerbate the computational cost issues due to GP and its particle degradation problem, we choose the EKF in this paper. The widely adopted EKF is a two-step version (one-step version can be seen in [49]), which is more numerically stable [50] and can handle irregular measurements. In each update, the two-step EKF propagates the state distribution and then corrects it with the current measurement, which are known as the prediction (time update) and correction (measurement update) steps, respectively. In the context of GPSSMs, considering the coupling between the system state and the GP, the distribution to be propagated and corrected is the joint distribution of both. These two operations can be expressed by:

$$p(\mathbf{x}_{t+1}, \mathbf{f} | \mathbf{y}_{1:t}) = \int p(\mathbf{x}_{t+1} | \mathbf{x}_t, \mathbf{f}) p(\mathbf{x}_t, \mathbf{f} | \mathbf{y}_{1:t}) d\mathbf{x}_t \quad (5)$$

$$p(\mathbf{x}_{t+1}, \mathbf{f} | \mathbf{y}_{1:t+1}) = \frac{p(\mathbf{y}_{t+1} | \mathbf{x}_{t+1}) p(\mathbf{x}_{t+1}, \mathbf{f} | \mathbf{y}_{1:t})}{p(\mathbf{y}_{t+1} | \mathbf{y}_{1:t})} \quad (6)$$

where $p(\mathbf{x}_{t+1} | \mathbf{x}_t, \mathbf{f})$ and $p(\mathbf{y}_{t+1} | \mathbf{x}_{t+1})$ are the transition and measurement densities as defined in (4), $p(\mathbf{x}_t, \mathbf{f} | \mathbf{y}_{1:t})$ denotes the joint posterior at time t , and $p(\mathbf{x}_{t+1}, \mathbf{f} | \mathbf{y}_{1:t})$ is the joint prior or predicted distribution at time $t + 1$. To evaluate the distribution in equations (5) and (6), the key challenges are the nonparametric nature of the GP and the nonlinearity in the transition and measurement models. Existing methods [40–44] typically first address the former by pre-parameterizing the GP into a fixed structure and then applying nonlinear filtering to handle the latter. However, pre-parameterization limits the operating domain, thus reducing the algorithm’s flexibility. To overcome this, we reverse the process: first handling the nonlinearity without any GP approximation, then addressing the nonparametric nature. We achieve the first procedure in the next subsection, resulting in an update equation with a factorized approximate distribution.

B. Factorized Approximate Distribution

To address the nonlinearity within the transition and measurement models, the following theorem is derived in this work by applying first-order linearization. To the best of our knowledge, this is the first time such a result has been derived.

Theorem 1. By approximating the transition and measurement models with first-order linearization, the approximate joint distribution between the state and GP, i.e. $q(\mathbf{x}_t, \mathbf{f}) \approx p(\mathbf{x}_t, \mathbf{f})$ in the prediction step (5) and correction step (6) follows the factorized form:

$$q(\mathbf{x}_t, \mathbf{f}) = p(\mathbf{f}_{\neq \mathbf{u}} | \mathbf{u}) q(\mathbf{x}_t, \mathbf{u}) \quad (7)$$

where $\mathbf{u} \triangleq \{u_i\}_{i=1}^{n_u}$ is a collection of a finite number of inducing points, $\mathbf{f}_{\neq \mathbf{u}}$ is the function values of the function $f(\cdot)$ except for \mathbf{u} , and $p(\mathbf{f}_{\neq \mathbf{u}} | \mathbf{u})$ is the exact GP conditional distribution similar to (2), namely,

$$p(\mathbf{f}_{\neq \mathbf{u}} | \mathbf{u}) = \mathcal{N} \left(\mathbf{K}_{\mathbf{f}_{\neq \mathbf{u}} \mathbf{u}} \mathbf{K}_{\mathbf{u} \mathbf{u}}^{-1} \mathbf{u}, \mathbf{K}_{\mathbf{f}_{\neq \mathbf{u}} \mathbf{f}_{\neq \mathbf{u}}} - \mathbf{K}_{\mathbf{f}_{\neq \mathbf{u}} \mathbf{u}} \mathbf{K}_{\mathbf{u} \mathbf{u}}^{-1} \mathbf{K}_{\mathbf{u} \mathbf{f}_{\neq \mathbf{u}}} \right) \quad (8)$$

and $q(\mathbf{x}_t, \mathbf{u})$ is a Gaussian distribution.

Given Theorem 1, since $p(\mathbf{f}_{\neq \mathbf{u}} | \mathbf{u})$ is known, we only need to update the finite-dimensional distribution $q(\mathbf{x}_t, \mathbf{u})$, which build a foundation for addressing the non-parametric nature of the GP. Moreover, the approximate joint distribution remains Gaussian, which can be evaluated using closed-form update equations. In the following, we will prove Theorem

1 and then derive these equations.

To facilitate the proof, we first introduce some notation regarding the approximate distributions $q(\mathbf{x}_t, \mathbf{u})$ and $q(\mathbf{x}_t, \mathbf{f})$. Specifically, these two distributions are expressed as:

$$\begin{aligned} q(\mathbf{x}_t, \mathbf{u}) &= \mathcal{N} \left(\begin{bmatrix} \mathbf{x}_t \\ \mathbf{u} \end{bmatrix} \middle| \begin{bmatrix} \boldsymbol{\mu}_t \\ \mathbf{m}_u \end{bmatrix}, \begin{bmatrix} \mathbf{P}_t & \mathbf{V}_{xu} \\ \mathbf{V}_{xu}^T & \mathbf{S}_{uu} \end{bmatrix} \right) \\ q(\mathbf{x}_t, \mathbf{f}) &= \mathcal{N} \left(\begin{bmatrix} \mathbf{x}_t \\ \mathbf{f} \end{bmatrix} \middle| \begin{bmatrix} \boldsymbol{\mu}_t \\ \mathbf{m}_f \end{bmatrix}, \begin{bmatrix} \mathbf{P}_t & \mathbf{V}_{xf} \\ \mathbf{V}_{xf}^T & \mathbf{S}_{ff} \end{bmatrix} \right) \end{aligned} \quad (9)$$

In this expression, the moments of the joint distribution are distinguished based on the state \mathbf{x}_t and inducing points \mathbf{u} or function values \mathbf{f} . For $q_t(\mathbf{x}_t, \mathbf{u})$, the vectors $\boldsymbol{\mu}_t = \mathbb{E}_{q(\mathbf{x}_t, \mathbf{u})}[\mathbf{x}_t]$ and $\mathbf{m}_u = \mathbb{E}_{q(\mathbf{x}_t, \mathbf{u})}[\mathbf{u}]$ represent the means of the state \mathbf{x}_t and the inducing points \mathbf{u} , respectively. $\mathbf{P}_t = \text{Var}_{q(\mathbf{x}_t, \mathbf{u})}[\mathbf{x}_t]$ denotes the autocovariance of \mathbf{x}_t , while $\mathbf{V}_{xu} = \text{Cov}_{q(\mathbf{x}_t, \mathbf{u})}[\mathbf{x}_t, \mathbf{u}]$ represents the cross-covariance between \mathbf{x}_t and \mathbf{u} , and $\mathbf{S}_{uu} = \text{Var}_{q(\mathbf{x}_t, \mathbf{u})}[\mathbf{u}]$ signifies the autocovariance of \mathbf{u} . For the moments of $q_t(\mathbf{x}_t, \mathbf{f})$, its notation follow the same logic, and the values are fully specified by the moments of $q(\mathbf{x}_t, \mathbf{u})$ given (7), specifically:

$$\begin{aligned} \mathbf{m}_f &= \mathbf{k}_{fu} \mathbf{m}_u \\ \mathbf{V}_{xf} &= \mathbf{V}_{xu} \mathbf{k}_{fu}^T \\ \mathbf{S}_{ff} &= \mathbf{K}_{ff} + \mathbf{k}_{fu} (\mathbf{S}_{uu} - \mathbf{K}_{uu}) \mathbf{k}_{fu}^T \end{aligned} \quad (10)$$

where we use the shorthand notation $\mathbf{k}_{fu} = \mathbf{K}_{fu} \mathbf{K}_{uu}^{-1}$. This equation can be easily derived by using (7) and the conditional distribution $p(\mathbf{f}|\mathbf{u})$ (8).

By means of the above notation, we will illustrate the proof of Theorem 1, which is based on mathematical induction. First, it can be demonstrated that at time 0, the joint distribution naturally satisfies the factorized form (7):

$$\begin{aligned} q(\mathbf{x}_0, \mathbf{f}) &\triangleq p(\mathbf{x}_0, \mathbf{f}) \\ &= p(\mathbf{f})p(\mathbf{x}_0) \\ &= p(\mathbf{f}_{\neq u}|\mathbf{u})p(\mathbf{u})p(\mathbf{x}_0) \\ &= p(\mathbf{f}_{\neq u}|\mathbf{u})q(\mathbf{x}_0, \mathbf{u}) \end{aligned} \quad (11)$$

where $q(\mathbf{x}_0, \mathbf{u}) \triangleq p(\mathbf{u})p(\mathbf{x}_0)$, $p(\mathbf{f})$ denotes the GP prior over all function values \mathbf{f} , and \mathbf{u} can be any collection of function values or an empty set. Therefore, the next step is to prove that the approximate updates of the prediction step (5) and the correction step (6) can preserve the factorized form.

For the prediction step, to address the nonlinearity in the transition model (4c), we employ first-order linearization

as in the EKF, specifically linearizing the transition model as follows:

$$\begin{aligned}
p(\mathbf{x}_{t+1}|\mathbf{x}_t, f) \\
&\approx \mathcal{N}\left(\mathbf{x}_{t+1} \middle| \mathbf{F}_t + \mathbf{A}_x(\mathbf{x}_t - \boldsymbol{\mu}_t) + \mathbf{A}_f(f_t - m_{f_t}), \boldsymbol{\Sigma}_p\right) \\
&\triangleq q(\mathbf{x}_{t+1}|\mathbf{x}_t, f_t).
\end{aligned} \tag{12}$$

where we use the notation for moments in (9) and the shorthand notation $f_t = f(\boldsymbol{\mu}_t)$, $m_{f_t} = \mathbb{E}_{q(\mathbf{x}_t, f)}[f_t]$, $\mathbf{F}_t = \mathbf{F}(\boldsymbol{\mu}_t, m_{f_t})$.

Additionally, the two Jacobian matrices in the equation are

$$\begin{aligned}
\mathbf{A}_f &= \left. \frac{\partial \mathbf{F}(\boldsymbol{\mu}_t, f)}{\partial f} \right|_{m_{f_t}} \\
\mathbf{A}_x &= \left. \frac{\partial \mathbf{F}(\mathbf{x}, m_{f(\mathbf{x})})}{\partial \mathbf{x}} \right|_{\boldsymbol{\mu}_t} = \left. \frac{\partial \mathbf{F}(\mathbf{x}, m_{f_t})}{\partial \mathbf{x}} \right|_{\boldsymbol{\mu}_t} + \mathbf{A}_f \left. \frac{\partial m_{f(\mathbf{x})}}{\partial \mathbf{x}} \right|_{\boldsymbol{\mu}_t}
\end{aligned} \tag{13}$$

where \mathbf{A}_f is the Jacobian matrix of the transition function \mathbf{F} with respect to the function value f evaluated at m_{f_t} , and \mathbf{A}_x is the Jacobian matrix of \mathbf{F} with respect to the state \mathbf{x} evaluated at $\boldsymbol{\mu}_t$, which includes both the direct effect of \mathbf{x} on \mathbf{F} and the indirect effect through the function value $f(\mathbf{x})$.

Note that, we use the hat notation $q(\mathbf{x}_{t+1}|\mathbf{x}_t, f_t)$ in (12) to denote the linearized model. As shown in (12), this linearized transition model depends solely on the function value f_t . Therefore, if we incorporate f_t into the inducing-point set, i.e., $\bar{\mathbf{u}} = [\mathbf{u}^T, f_t^T]^T$, the prediction result in (5) by using the linearized model (12) retains the factorized form (7):

$$\begin{aligned}
q^-(\mathbf{x}_{t+1}, f) &= \int q(\mathbf{x}_t, f) q(\mathbf{x}_{t+1}|\mathbf{x}_t, f_t) d\mathbf{x}_t \\
&= p(f_{\neq \bar{\mathbf{u}}}|\bar{\mathbf{u}}) \int q(\mathbf{x}_t, \bar{\mathbf{u}}) q(\mathbf{x}_{t+1}|\mathbf{x}_t, f_t) d\mathbf{x}_t \\
&= p(f_{\neq \bar{\mathbf{u}}}|\bar{\mathbf{u}}) q^-(\mathbf{x}_{t+1}, \bar{\mathbf{u}})
\end{aligned} \tag{14}$$

where we use the superscript "-" to denote predicted distributions, and $q^-(\mathbf{x}_{t+1}, \bar{\mathbf{u}}) = \int q(\mathbf{x}_t, \bar{\mathbf{u}}) q(\mathbf{x}_{t+1}|\mathbf{x}_t, f_t) d\mathbf{x}_t$. It can be observed that the factorized form is preserved at the cost of augmenting the inducing-point set, an inevitable consequence of the non-parametric nature of the GP. This increase in the number of inducing points will lead to a rapid rise in computational burden, rendering inference intractable, which will be addressed in Section IV.A.

For the correction step, the derivation is similar. To handle the nonlinearity in the measurement model (4d), the first-order linearization is used again:

$$\begin{aligned}
p(\mathbf{y}_{t+1}|\mathbf{x}_{t+1}) \\
&\approx \mathcal{N}\left(\mathbf{y}_{t+1} \middle| \mathbf{g}(\boldsymbol{\mu}_{t+1}^-) + \mathbf{C}_x(\mathbf{x}_{t+1} - \boldsymbol{\mu}_{t+1}^-), \boldsymbol{\Sigma}_m\right) \\
&\triangleq q(\mathbf{y}_{t+1}|\mathbf{x}_{t+1})
\end{aligned} \tag{15}$$

where $\mu_{t+1}^- = \mathbb{E}_{q^-(\mathbf{x}_{t+1}, \bar{\mathbf{u}})}[\mathbf{x}_{t+1}]$ denotes the predicted mean of state \mathbf{x}_{t+1} and the measurement Jacobian is $\mathbf{C}_x = \partial \mathbf{g}(\mathbf{x}) / \partial \mathbf{x} \big|_{\mu_{t+1}^-}$. By incorporating the linearized measurement model $q(\mathbf{y}_{t+1} | \mathbf{x}_{t+1})$ into the correction step (6), the factorized form can be retained as follows:

$$\begin{aligned} q(\mathbf{x}_{t+1}, \mathbf{f}) &\propto q^-(\mathbf{x}_{t+1}, \mathbf{f}) q(\mathbf{y}_{t+1} | \mathbf{x}_{t+1}) \\ &= p(\mathbf{f}_{\neq \bar{\mathbf{u}}} | \bar{\mathbf{u}}) q^-(\mathbf{x}_{t+1}, \bar{\mathbf{u}}) q(\mathbf{y}_{t+1} | \mathbf{x}_{t+1}) \\ &\propto p(\mathbf{f}_{\neq \bar{\mathbf{u}}} | \bar{\mathbf{u}}) q(\mathbf{x}_{t+1}, \bar{\mathbf{u}}) \end{aligned} \quad (16)$$

where $q(\mathbf{x}_{t+1}, \bar{\mathbf{u}}) \propto q^-(\mathbf{x}_{t+1}, \bar{\mathbf{u}}) q(\mathbf{y}_{t+1} | \mathbf{x}_{t+1})$.

Thus far, we have proven Theorem 1, in which only first-order linearization is used and the inducing-point set is continually expanded to match the data distribution. In the derivation, we also obtain the approximate prediction equation (14) and correction equation (16) for the joint distribution $q(\mathbf{x}_t, \mathbf{f})$, which can be used to derive practical update equations for it. It is evident that the joint distribution $q(\mathbf{x}_t, \mathbf{u})$ contains the essential information of $q(\mathbf{x}_t, \mathbf{f})$ and thus is the only component that requires updating. Given that $q(\mathbf{x}_t, \mathbf{u})$ is Gaussian, we only need to derive its moment matching equations, which are presented in the next subsection.

C. Moment Matching Equation

For simplicity in the moment matching equation, we define the union of the system state \mathbf{x}_t and inducing points \mathbf{u} as an augmented state, i.e., $\mathbf{X}_t = [\mathbf{x}_t^T, \mathbf{u}^T]^T$. Consequently, the approximate distribution $q(\mathbf{x}_t, \mathbf{u})$ can be expressed as $q(\mathbf{X}_t)$, with its mean and covariance denoted as $\xi_t = \mathbb{E}_{q(\mathbf{X}_t)}[\mathbf{X}_t]$ and $\Sigma_t = \text{Var}_{q(\mathbf{X}_t)}[\mathbf{X}_t]$, respectively. Based on this definition, the moment matching equation becomes a recursive equation for ξ_t and Σ_t .

For the prediction step, given the update equation (14), we should first add the point f_t into the inducing point set \mathbf{u} , thus obtaining the new set $\bar{\mathbf{u}}$. Therefore, we define the new augmented state $\bar{\mathbf{X}}_t = [\mathbf{x}_t^T, \bar{\mathbf{u}}^T]^T$, similar to \mathbf{X}_t . Correspondingly, we have the approximate distribution $q(\bar{\mathbf{X}}_t)$ with mean $\bar{\xi}_t$ and covariance $\bar{\Sigma}_t$, which can be evaluated using (9) and (10) by letting $\mathbf{f} = \bar{\mathbf{u}}$. Then, by applying the update equation (14), the moment matching equation for the prediction step can be easily derived, with a result similar to that of the EKF:

$$\begin{aligned}
\bar{\xi}_{t+1}^- &= [F_t^T, m_u^T]^T \\
\bar{\Sigma}_{t+1}^- &= \Phi \bar{\Sigma}_t \Phi^T + \Sigma_{f, \bar{X}} \\
\Phi &= \begin{bmatrix} A_x & \mathbf{0} & A_f \\ \mathbf{0} & I_{n_u} & \mathbf{0} \\ \mathbf{0} & \mathbf{0} & 1 \end{bmatrix} \\
\Sigma_{f, \bar{X}} &= \begin{bmatrix} \Sigma_p & \mathbf{0} \\ \mathbf{0} & \mathbf{0} \end{bmatrix}
\end{aligned} \tag{17}$$

where $\bar{\xi}_{t+1}^-$ and $\bar{\Sigma}_{t+1}^-$ represent the predicted mean and covariance for the augmented state \bar{X}_{t+1} . Φ denotes the transition Jacobian matrix for \bar{X}_{t+1} , $\Sigma_{f, \bar{X}}$ is the process noise covariance for \bar{X}_{t+1} , and I_{n_u} is the identity matrix.

For the correction step, the moment matching equation can be easily obtained using the approximate correction equation in (16), with the result as follows:

$$\begin{aligned}
H &= \begin{bmatrix} C_x & \mathbf{0} \end{bmatrix} \\
G &= \bar{\Sigma}_{t+1}^- H^T \left(C_x P_{t+1}^- C_x^T + \Sigma_m \right)^{-1} \\
\bar{\xi}_{t+1} &= \bar{\xi}_{t+1}^- + G [y_{t+1} - g(\mu_{t+1}^-)] \\
\bar{\Sigma}_{t+1} &= \bar{\Sigma}_{t+1}^- - G H \bar{\Sigma}_{t+1}^-
\end{aligned} \tag{18}$$

where P_{t+1}^- denotes the predicted variance of the system state x_{t+1} , $\bar{\xi}_{t+1}$ and $\bar{\Sigma}_{t+1}$ represent the posterior mean and covariance for the augmented state \bar{X}_{t+1} , H is its measurement Jacobian, and G corresponds to the Kalman gain. Therefore, through the moment matching equations (17) and (18), closed-form recursive inference for online GPSSMs can be achieved.

In summary, this section presents a two-step Bayesian update framework for online GPSSMs, in which first-order linearization is employed to address the nonlinearity in both the transition and measurement models. By applying linearization and expanding the inducing-point set, the joint distribution maintains a factorized form, which leads directly to the moment matching equations (17) and (18). Linearization is a key step in this method, providing accurate approximations when the system exhibits mild nonlinearity and the variance of the joint distribution is small. This approximation is similar to that used in the EKF, and some techniques can be transferred to the proposed method, such as adding a positive-definite term to the process noise covariance to enhance robustness. Although first-order linearization may be insufficient in some cases, the above derivation establishes a general framework in which other advanced nonlinear filtering techniques can be incorporated by replacing the EKF-based moment matching.

In theory, the derived equations have enabled recursive learning for GPSSMs without being restricted by the operating domain. However, as discussed in Section III.B, the increasing number of inducing points significantly raises the computational burden for moment evaluation, which will make inference intractable. In the next section, an approximation method will be introduced to address this issue.

IV. Adaptation of Inducing points and Hyperparameters

While the recursive learning algorithm for GPSSMs has been developed, two issues remain: the computational burden problem due to the non-parameteric nature of GP, and the hyperparameter online adaptation problem. In Section IV.A, a inducing point set adjustment algorithm is introduced to maintain limited computational complexity, and in Section IV.B, an online hyperparameter adaptation method is derived to improve learning accuracy.

A. Dynamic Adjusting the Inducing Points Set

As discussed in Section III, the computational cost of the learning algorithm increases with the addition of inducing points. This challenge is also encountered in the development of kernel-based online regression algorithms, such as Kernel Recursive Least Squares (KRLS) [51] and Sparse Online Gaussian Processes (SOGP) [27, 52]. These two methods are equivalent to some extent and control computational cost by limiting the size of the inducing point set to a predefined budget M . Specifically, this strategy is achieved through two operations: discarding the least important point when the set exceeds the budget M , and adding only sufficiently novel points. To implement the discarding and adding operations, the following two key problems must be addressed: (1) how to remove a point with minimal accuracy loss, and (2) how to evaluate the importance or novelty of a point. In the following, we will address these two problems in the context of GPSSMs and develop an adjustment method for the inducing point set, thereby overcoming the computational burden issue. For convenience, let u_d denote the inducing point to be discarded, with index i_d in the point set, and let \mathbf{u}_1 represent the inducing points left.

For the first problem, we define that, after discarding point u_d , the new joint distribution $\hat{q}(\mathbf{x}, \mathbf{f})$, still retains the factorized form (7), namely,

$$\hat{q}(\mathbf{x}, \mathbf{f}) = p(\mathbf{f}_{\neq u_1} | \mathbf{u}_1) \hat{q}(\mathbf{x}, \mathbf{u}_1) \quad (19)$$

where $p(\mathbf{f}_{\neq u_1} | \mathbf{u}_1)$ is the conditional prior (8), and $\hat{q}(\mathbf{x}, \mathbf{u}_1)$ is defined to be Gaussian for achieving closed-form implementation. Then, to ensure minimal accuracy loss, we can seek the optimal solution within the distribution family of $\hat{q}(\mathbf{x}, \mathbf{f})$, such that the distance between it and the original joint distribution $q(\mathbf{x}, \mathbf{f}) = p(\mathbf{f}_{\neq u_1} | \mathbf{u}_1) q(\mathbf{x}, \mathbf{u})$ is minimized. Since $\hat{q}(\mathbf{x}, \mathbf{u}_1)$ controls the approximate distribution $\hat{q}(\mathbf{x}, \mathbf{f})$, it is sufficient to find the optimal distribution for $\hat{q}(\mathbf{x}, \mathbf{u}_1)$. Here, we use the inclusive KL divergence as a distance metric, namely $\text{KL}[q \| \hat{q}] = \int q \log(q/\hat{q})$, which

results in a simple optimal distribution:

$$\begin{aligned}
\hat{q}^*(\mathbf{x}, \mathbf{u}_1) &= \arg \min_{\hat{q}(\mathbf{x}, \mathbf{u}_1)} \text{KL} [q(\mathbf{x}, \mathbf{f}) \| \hat{q}(\mathbf{x}, \mathbf{f})] \\
&= \arg \min_{\hat{q}(\mathbf{x}, \mathbf{u}_1)} \text{KL} [p(\mathbf{f}_{\neq u} | \mathbf{u}) q(\mathbf{x}, \mathbf{u}) \| p(\mathbf{f}_{\neq u_1} | \mathbf{u}_1) \hat{q}(\mathbf{x}, \mathbf{u}_1)] \\
&= \arg \min_{\hat{q}(\mathbf{x}, \mathbf{u}_1)} \text{KL} [q(\mathbf{x}, \mathbf{u}) \| p(u_d | \mathbf{u}_1) \hat{q}(\mathbf{x}, \mathbf{u}_1)] \\
&= \int q(\mathbf{x}, \mathbf{u}) d\mathbf{u}_d
\end{aligned} \tag{20}$$

It can be observed that the optimal distribution $\hat{q}^*(\mathbf{x}, \mathbf{u}_1)$ only involves marginalizing the discarded inducing point u_d from the original distribution. Through (20), optimal deletion for a given inducing point can be achieved.

Furthermore, for the second problem, the importance or novelty of a point can be assessed by the accuracy loss incurred from optimally discarding it. Specifically, this can be done by calculating the KL divergence in (20) with $\hat{q}(\mathbf{x}, \mathbf{u}_1) = \hat{q}^*(\mathbf{x}, \mathbf{u}_1)$:

$$\begin{aligned}
D^* &= \text{KL} [q(\mathbf{x}, \mathbf{u}) \| p(u_d | \mathbf{u}_1) \hat{q}^*(\mathbf{x}, \mathbf{u}_1)] \\
&= D_1 - D_2 - D_3 \\
D_1 &= \int q(\mathbf{x}, \mathbf{u}) \log q(\mathbf{x}, \mathbf{u}) d\mathbf{x} d\mathbf{u} \\
D_2 &= \int q(\mathbf{u}) \log p(u_d | \mathbf{u}_1) d\mathbf{u} \\
D_3 &= \int \hat{q}^*(\mathbf{x}, \mathbf{u}_1) \log \hat{q}^*(\mathbf{x}, \mathbf{u}_1) d\mathbf{u}_1
\end{aligned} \tag{21}$$

Through the KL divergence D^* , the accuracy loss from discarding the inducing point u_d can be evaluated. A computable score s_d quantifying the accuracy loss can be obtained by dropping the u_d -irrelevant terms in (21) (the derivation is deferred to Appendix VII.A), namely:

$$\begin{aligned}
s_d &= \Delta_1 + \Delta_2 + \Delta_3 \\
\Delta_1 &= \mathbf{m}_u^T \mathbf{Q}_{du}^T \mathbf{Q}_{dd}^{-1} \mathbf{Q}_{du} \mathbf{m}_u \\
\Delta_2 &= \text{tr} \left(\mathbf{Q}_{du} \mathbf{S}_{uu} \mathbf{Q}_{du}^T \mathbf{Q}_{dd}^{-1} \right) \\
\Delta_3 &= \log |\mathbf{\Omega}_{dd}| - \log |\mathbf{Q}_{dd}|
\end{aligned} \tag{22}$$

where we denote the inverse of the joint covariance as $\mathbf{\Omega} = \mathbf{\Sigma}_t^{-1}$, and $\mathbf{\Omega}_{dd}$ is the element of the matrix $\mathbf{\Omega}$ corresponding to the discarded point u_d , namely, its $(d_x + i_d)$ -th diagonal element. In addition, \mathbf{Q}_{dd} and \mathbf{Q}_{du} are the i_d -th diagonal element and the i_d -th row of the inverse kernel matrix $\mathbf{Q} = \mathbf{K}_{uu}^{-1}$. Among the terms in (22), Δ_1 represents the accuracy loss in the mean of the joint distribution $q(\mathbf{x}_t, \mathbf{f})$, which matches the result in KRLS [51], while Δ_2 and Δ_3 correspond to the loss in the covariance, which achieve more precise quantification and were not derived in KRLS [51]. Overall, the

score s_d quantifies the relative accuracy loss from discarding u_d , with a smaller score indicating a smaller accuracy loss.

Through (20) and (22), we have addressed the two key challenges. Based on these, we can provide the adjustment rule for the inducing point set, which is divided into discarding and adding operations. For the discarding operation, the rule is as follows: if the size of the inducing point set exceeds the budget M , evaluate the score of each point using (22) and remove the one with the lowest score. According to (20), the moments of the new joint distribution $\hat{q}^*(\mathbf{x}, \mathbf{u}_1)$ can be easily evaluated by deleting the corresponding elements associated with u_d from the original moments.

For the adding operation, as in the KRLS [51], we will use a more intuitive metric for selecting points, which is derived from the score in (22). Specifically, by observing the score s_d in (22), it can be seen that if $\mathbf{Q}_{dd}^{-1} \rightarrow 0$, the score will approach its minimum value, i.e., $s_d \rightarrow -\infty$, indicating that the accuracy loss from deleting u_d approaches 0. According to the matrix inversion formula (see Appendix A of [52]), $\mathbf{Q}_{dd}^{-1} = \mathbf{K}_{dd} - \mathbf{K}_{dl}\mathbf{K}_{ll}^{-1}\mathbf{K}_{ld}$, where subscripts d and l corresponding to u_d and \mathbf{u}_1 , and \mathbf{Q}_{dd}^{-1} actually is the GP prior conditional variance of u_d given \mathbf{u}_1 according to (8). Therefore, we can use the GP prior conditional variance of f_t given the current inducing points \mathbf{u} as the metric for novelty, namely:

$$\gamma = \mathbf{K}_{tt} - \mathbf{K}_{tu}\mathbf{K}_{uu}^{-1}\mathbf{K}_{ut} \quad (23)$$

where subscript t denotes f_t . Then, if γ is less than a certain threshold, denoted as ε_{tol} , we will not add the new point to the inducing point set. This filtering process helps to slow down the increase in the size of the inducing point set. Besides, more importantly, it plays a crucial role in ensuring the numerical stability of the learning algorithm. Specifically, when γ is small, adding a new point can cause the updated kernel matrix $\mathbf{K}_{\tilde{u}\tilde{u}}$ to approach singularity, which would negatively affect the stability of the algorithm. Therefore, the value of the threshold ε_{tol} for adding a point can be determined based on the machine accuracy. Accordingly, when not adding points, the moment updating equation (17) will be modified. We derive this equation in Appendix VII.B, whose result is;

$$\begin{aligned} \xi_{t+1}^- &= [\mathbf{F}_t^T, \mathbf{m}_u^T]^T \\ \Sigma_{t+1}^- &= \Phi \Sigma_t \Phi^T + \Sigma_{p,X} \\ \Phi &= \begin{bmatrix} \mathbf{A}_x & \mathbf{A}_f \mathbf{k}_{tu} \\ \mathbf{0} & \mathbf{I}_{n_u} \end{bmatrix} \\ \Sigma_{p,X} &= \begin{bmatrix} \mathbf{A}_f \gamma \mathbf{A}_f^T + \Sigma_p & \mathbf{0} \\ \mathbf{0} & \mathbf{0} \end{bmatrix} \end{aligned} \quad (24)$$

This equation is similar to the original equation (17), differing only in the expression for the transition Jacobian Φ and the process noise covariance $\Sigma_{p,X}$.

In summary, this subsection derives the optimal deletion method for inducing points and presents a metric for quantifying the importance or novelty of points. Based on these, a dynamic adjustment algorithm, including discarding and adding operations for the inducing point set, is developed to ensure limited computational cost and algorithm stability. In the next subsection, we will address the online hyperparameter optimization problem to enhance learning accuracy.

B. Online Optimization of GP Hyperparameters

In GP learning, if the hyperparameters θ significantly mismatch the function to be learned, it will result in substantial learning errors. In offline learning, the hyperparameters θ can be optimized using data by maximizing the log marginal likelihood [15]. However, as illustrated in the Introduction, the online setting presents two challenges for hyperparameter optimization: 1) the information source problem due to the lack of data retention, and 2) the coupling between GP hyperparameters and the posterior distribution. In this subsection, we will address these two challenges and propose an online GP hyperparameter optimization method for GPSSMs. For clarity, we denote the quantities corresponding to before and after hyperparameter optimization with the superscripts or subscripts "old" and "new", respectively. Additionally, to highlight the impact of the GP hyperparameters, probability distributions depending on θ will be rewritten as $p(\cdot; \theta)$.

Firstly, to find the information source for hyperparameters optimization, we can first observe the expression of the exact joint posterior distribution, which is given as follows for time t :

$$p(\mathbf{x}_t, \mathbf{f} | \mathbf{y}_{1:t}; \theta) = \frac{p(\mathbf{f}; \theta) p(\mathbf{x}_t, \mathbf{y}_{1:t} | \mathbf{f})}{p(\mathbf{y}_{1:t}; \theta)} \quad (25)$$

where $p(\mathbf{f}; \theta)$ denotes the GP prior on function values \mathbf{f} , and the likelihood model $p(\mathbf{x}_t, \mathbf{y}_{1:t} | \mathbf{f}) = \int \prod_{i=1}^t p(\mathbf{y}_i, \mathbf{x}_i | \mathbf{x}_{i-1}, \mathbf{f}) p(\mathbf{x}_0) d\mathbf{x}_{0:t-1}$. By using this likelihood model, we can evaluate the marginal likelihood $p(\mathbf{y}_{1:t}; \theta) = \int p(\mathbf{f}; \theta) p(\mathbf{x}_t, \mathbf{y}_{1:t} | \mathbf{f}) d\mathbf{x}_t d\mathbf{f}$, and then optimize the GP hyperparameters by maximizing it. However, for online hyperparameter optimization, an explicit likelihood model is unavailable because the past measurements $\mathbf{y}_{1:t-1}$ are not stored. Instead, we only have an approximation of the left-hand side of (25), namely the approximate distribution corresponding to the old hyperparameters θ_{old} :

$$q_{\text{old}}(\mathbf{x}_t, \mathbf{f}) \approx p(\mathbf{x}_t, \mathbf{f} | \mathbf{y}_{1:t}; \theta_{\text{old}}) \quad (26)$$

Fortunately, by observing (25), it can be found that the likelihood model can be implicitly obtained by:

$$\begin{aligned} p(\mathbf{x}_t, \mathbf{y}_{1:t} | \mathbf{f}) &= \frac{p(\mathbf{x}_t, \mathbf{f} | \mathbf{y}_{1:t}; \theta_{\text{old}}) p(\mathbf{y}_{1:t}; \theta_{\text{old}})}{p(\mathbf{f}; \theta_{\text{old}})} \\ &\approx \frac{q_{\text{old}}(\mathbf{x}_t, \mathbf{f}) p(\mathbf{y}_{1:t}; \theta_{\text{old}})}{p(\mathbf{f}; \theta_{\text{old}})} \end{aligned} \quad (27)$$

In other words, the measurement information is distilled into the approximate distribution $q_{old}(\mathbf{x}_t, \mathbf{f})$ and the latter can recover the likelihood model, thereby addressing the information source problem.

Secondly, utilizing the information source in (27), we can find the optimization objective for GP hyperparameters and evaluate the posterior distribution after hyperparameter optimization. The key idea in achieving this is to evaluate the joint probability model $p(\mathbf{f}; \boldsymbol{\theta})p(\mathbf{x}_t, \mathbf{y}_{1:t}|\mathbf{f})$, which is proportional to the posterior distribution, and its integral is the marginal likelihood that can serve as the objective function. For convenience, we actually derive the posterior distribution first, which can be obtained by combining the expression of the posterior distribution (25) with the approximate likelihood model (27), namely:

$$\begin{aligned}
& p(\mathbf{x}_t, \mathbf{f}|\mathbf{y}_{1:t}; \boldsymbol{\theta}_{new}) \\
&= \frac{p(\mathbf{f}; \boldsymbol{\theta}_{new})p(\mathbf{x}_t, \mathbf{y}_{1:t}|\mathbf{f})}{p(\mathbf{y}_{1:t}; \boldsymbol{\theta}_{new})} \\
&\approx \frac{p(\mathbf{f}; \boldsymbol{\theta}_{new})q_{old}(\mathbf{x}_t, \mathbf{f})p(\mathbf{y}_{1:t}; \boldsymbol{\theta}_{old})}{p(\mathbf{y}_{1:t}; \boldsymbol{\theta}_{new})p(\mathbf{f}; \boldsymbol{\theta}_{old})} \\
&\triangleq q_{new}(\mathbf{x}_t, \mathbf{f})
\end{aligned} \tag{28}$$

where $q_{new}(\mathbf{x}_t, \mathbf{f})$ denotes the approximate joint distribution corresponding to the new hyperparameters $\boldsymbol{\theta}_{new}$. In (28), since the distributions $p(\mathbf{f}; \boldsymbol{\theta}_{old})$, $p(\mathbf{f}; \boldsymbol{\theta}_{new})$, and $q_{old}(\mathbf{x}_t, \mathbf{f})$ are all Gaussian, the new approximate distribution $q_{new}(\mathbf{x}_t, \mathbf{f})$ is also Gaussian. By expanding the distribution related to \mathbf{f} in the third row of (28) with the conditional distribution $p(\mathbf{f}|\mathbf{u})$, it can be shown that the new distribution retains the factorized form $q_{new}(\mathbf{x}_t, \mathbf{f}) = p(\mathbf{f}_{\neq \mathbf{u}}|\mathbf{u}; \boldsymbol{\theta}_{new})q_{new}(\mathbf{x}_t, \mathbf{u})$, where:

$$\begin{aligned}
q_{new}(\mathbf{x}_t, \mathbf{u}) &= \frac{p(\mathbf{u}; \boldsymbol{\theta}_{new})q_{old}(\mathbf{x}_t, \mathbf{u})p(\mathbf{y}_{1:t}; \boldsymbol{\theta}_{old})}{p(\mathbf{y}_{1:t}; \boldsymbol{\theta}_{new})p(\mathbf{u}; \boldsymbol{\theta}_{old})} \\
&\propto \frac{p(\mathbf{u}; \boldsymbol{\theta}_{new})q_{old}(\mathbf{x}_t, \mathbf{u})}{p(\mathbf{u}; \boldsymbol{\theta}_{old})}
\end{aligned} \tag{29}$$

Therefore, we can obtain the new posterior distribution after the GP hyperparameters change.

Furthermore, by integrating both sides of the first row of (29), we can obtain the marginal likelihood for hyperparameter optimization, which leads to:

$$\frac{p(\mathbf{y}_{1:t}; \boldsymbol{\theta}_{new})}{p(\mathbf{y}_{1:t}; \boldsymbol{\theta}_{old})} = \int \frac{p(\mathbf{u}; \boldsymbol{\theta}_{new})q_{old}(\mathbf{x}_t, \mathbf{u})}{p(\mathbf{u}; \boldsymbol{\theta}_{old})} d\mathbf{x}_t d\mathbf{u} \tag{30}$$

Based on these results, the practical optimization objective and moment matching equation for the posterior distribution can be derived, which are presented below.

First, by eliminating some $\boldsymbol{\theta}_{new}$ -irrelevant terms in (30) (see Appendix VII.C), a practical optimization objective for GP hyperparameters is to minimize:

$$\begin{aligned}
\mathcal{L} &= \mathcal{L}_1 + \mathcal{L}_2 \\
\mathcal{L}_1 &= (\mathbf{m}_u^{\text{old}})^T (\mathbf{S}_{uu}^{\text{old}} + \Delta \mathbf{K})^{-1} \mathbf{m}_u^{\text{old}} \\
\mathcal{L}_2 &= \log |\mathbf{K}_{uu}^{\text{new}} + [\mathbf{I}_{n_u} - \mathbf{K}_{uu}^{\text{new}} (\mathbf{K}_{uu}^{\text{old}})^{-1}] \mathbf{S}_{uu}^{\text{old}}| \\
\Delta \mathbf{K} &= [(\mathbf{K}_{uu}^{\text{new}})^{-1} - (\mathbf{K}_{uu}^{\text{old}})^{-1}]^{-1}
\end{aligned} \tag{31}$$

where $\mathbf{K}_{uu}^{\text{new}}$ and $\mathbf{K}_{uu}^{\text{old}}$ denote the kernel matrix of \mathbf{u} evaluated with new and old GP hyperparameters. Therefore, the GP hyperparameters can be optimized online by implementing gradient descent on the loss function (31) in each algorithm iteration. Since the approximate posterior $q(\mathbf{x}, \mathbf{f})$ retains the measurement information, it is not necessary to optimize to convergence in a single algorithm iteration.

Second, the moments of the new posterior $q_{\text{new}}(\mathbf{x}_t, \mathbf{u})$ after the hyperparameter update can be evaluated using a Kalman filter-like equation (derivation in Appendix VII.C):

$$\begin{aligned}
\tilde{\mathbf{H}} &= \begin{bmatrix} \mathbf{0} & \mathbf{I}_{n_u} \end{bmatrix} \\
\tilde{\mathbf{G}} &= \Sigma_t^{\text{old}} \tilde{\mathbf{H}}^T (\mathbf{S}_{uu}^{\text{old}} + \Delta \mathbf{K})^{-1} \\
\xi_t^{\text{new}} &= \xi_t^{\text{old}} - \tilde{\mathbf{G}} \xi_t^{\text{old}} \\
\Sigma_t^{\text{new}} &= \Sigma_t^{\text{old}} - \tilde{\mathbf{G}} \tilde{\mathbf{H}} \Sigma_t^{\text{old}}
\end{aligned} \tag{32}$$

In summary, by recovering an approximate likelihood model from the current filtering distribution, this subsection derives the objective function and posterior update equation for online hyperparameter optimization. This method reduces the burden of hyperparameter tuning at the learning initialization stage and improves online learning accuracy by adjusting the GP prior to match the actual function characteristics.

Remark IV.1. The online optimization method for GP hyperparameters most closely related to this paper is [29], an online GPR method. In this method, the likelihood model is similarly recovered from the approximate posterior distribution, and it is used to optimize the location of inducing points and GP hyperparameters. Clearly, in GPSSMs, it is possible to optimize the inducing inputs in the same way. However, we do not pursue this approach because simultaneously optimizing the inducing inputs and hyperparameters would complicate the loss function and the adjustment equation for the posterior distribution. Additionally, we observe that in GPSSMs, due to the system states being implicitly measured, the difficulty of optimizing the inducing inputs increases. Therefore, we separate the optimization of inducing inputs and GP hyperparameters and determine the inducing-point set using a discretized selection method.

C. Algorithm Summary

In summary, we have addressed the four challenges outlined in the Introduction for implementing online GPSSMs. Specifically, first, nonlinearity and coupling are handled through first-order linearization and joint inference of the system state and GP, leading to a closed-form Bayesian update equation. Second, a dynamic inducing-point adjustment algorithm is developed to overcome the computational burden caused by the non-parametric nature of the GP. Third, we recover the likelihood model from the approximate posterior distribution and utilize it for the online optimization of GP hyperparameters, thus enhancing learning accuracy. Based on these solutions, we have developed an efficient online GPSSM method that can adapt to both the operating domain and GP hyperparameters. Due to its flexible recursive inference capability for GPSSMs, this method is referred to as the recursive GPSSM (RGPSSM), which is summarized in Algorithm 1. A schematic diagram of the algorithmic workflow is shown in Fig. 1.

Algorithm 1 Recursive Gaussian Process State Space Model (RGPSSM)

Input: initial inducing points \mathbf{u} , threshold for adding points ε_{tol} , budget for the inducing-point set M .

- 1: **repeat**
- 2: Assess the novelty γ of the new point f_t using (23).
- 3: **if** $\gamma > \varepsilon_{tol}$ **then**
- 4: Add f_t to the inducing-point set and propagate the moments using (17).
- 5: **else**
- 6: Propagate the moments using (24).
- 7: **end if**
- 8: **if** the number of inducing points $n_u > M$ **then**
- 9: Identify the least important point based on the score in (22) and remove it using (20).
- 10: **end if**
- 11: **if** a new measurement y_t is available **then**
- 12: Correct the moments using (18).
- 13: **end if**
- 14: Minimize \mathcal{L} in (31) to update the GP hyperparameters θ using the Adam optimizer [53], and subsequently update the moments using (32).
- 15: **until** operation ends

In theory, Algorithm 1 has the recursive learning capability for GPSSMs; however, as with the Kalman filter, there are numerical stability issues when implemented on a computer. Specifically, the algorithm requires the propagation of the covariance matrix Σ_t of the augmented state \mathbf{X}_t , which can easily lose positive definiteness due to the accumulation of rounding errors. To address this problem, a stable implementation based on Cholesky factorization is derived, as detailed in Appendix VII.D. This implementation method is capable of enhancing the numerical stability by making the computation more compact. In the next section, we will discuss the computational complexity of the Cholesky version of RGPSSM, along with the extension to the multi-output GP cases.

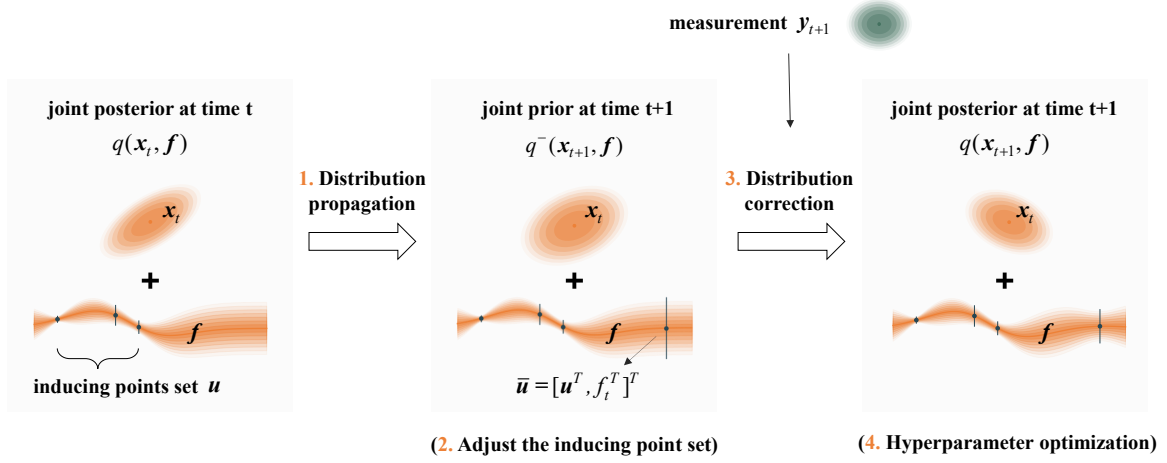


Fig. 1 Schematic diagram of the RGPSSM algorithmic workflow.

V. Extension to Multi-output GP and Discussion

This section extends the single-output GP version of the RGPSSM method to the multi-output GP case, and systematically analyzes the computational complexity, generalization, and potential of the proposed method.

A. Multi-output GP Version

In numerous practical applications, the unknown function to be learned within SSMs exhibits multiple outputs, represented as $f(\cdot) : \mathbb{R}^{d_x} \rightarrow \mathbb{R}^{d_f}$ where $d_f > 1$. To accommodate this multi-output nature, the GP modeling for $f(\cdot)$ must be extended to a multi-output form, necessitating a modification of the kernel function $K_0(\cdot, \cdot)$ to yield a $d_f \times d_f$ matrix output. For this purpose, we employ a straightforward multi-output kernel formulation, expressed as:

$$K_0(\cdot, \cdot) = K_0(\cdot, \cdot) \Xi \quad (33)$$

where $K_0(\cdot, \cdot)$ in the RHS represents the single-output kernel, and Ξ denotes the signal covariance between each function output dimension. Based on this multi-output kernel function, the kernel matrix has a Kronecker product structure, i.e., $K_0(\mathcal{X}_1, \mathcal{X}_2) = K_0(\mathcal{X}_1, \mathcal{X}_2) \otimes \Xi$. This structure indicates that the (i, j) -th $d_f \times d_f$ block of the kernel matrix $K_0(\mathcal{X}_1, \mathcal{X}_2)$ is the prior covariance between function values $f(\mathbf{x}_i)$ and $f(\mathbf{x}_j)$. Therefore, the only modification from the single-output GP version of RGPSSM to the multi-output GP version is to convert scalar elements in related vectors or matrices into corresponding blocks, which are presented in the following.

Firstly, the moments of joint distribution $q(\mathbf{x}, \mathbf{u})$ including mean \mathbf{m}_u , cross-covariance \mathbf{V}_{xu} and auto-covariance \mathbf{S}_{uu} have new definitions. Specifically,

- The i -th column block (with shape $d_f \times 1$) of column vector \mathbf{m}_u represents the mean of the inducing point \mathbf{u}_i
- The i -th row block (with shape $d_x \times d_f$) of matrix \mathbf{V}_{xu} represents the cross-covariance between state \mathbf{x} and the inducing point \mathbf{u}_i
- The (i, j) -th block (with shape $d_f \times d_f$) of matrix \mathbf{S}_{uu} represents the cross-covariance between the inducing points \mathbf{u}_i and \mathbf{u}_j

Secondly, among the inducing point management, the calculation of the score s_d and novelty γ require updates. For the evaluation of the score s_d in (22), the modifications only involve updating the definitions of several quantities:

- \mathbf{Q}_{du} is the i_d -th row block of \mathbf{Q}
- \mathbf{Q}_{dd} is the i_d -th diagonal block of \mathbf{Q}
- $\mathbf{\Omega}_{dd}$ is the i_d -th diagonal block of the inducing points submatrix in $\mathbf{\Omega}$, where the inducing points submatrix is defined as the matrix slice $\mathbf{\Omega}[d_x :, d_x :]$

For the criterion of adding points, since $\boldsymbol{\gamma}$ in (23) is now a matrix, the criterion is modified to $\text{tr}(\boldsymbol{\gamma}) > \varepsilon_{tol}$. Additionally, when adding or removing inducing points, the updates to the moments are performed in a block-wise manner based on the new definitions.

Overall, the extension to the multi-output GP version is straightforward, with modifications involving the kernel function, the definitions of some vectors and matrices, and the evaluation criteria for inducing points management. It is evident that the dimensions of statistical moments will scale with the dimension of GP output, thus impacting the computational complexity, which is analyzed in the next subsection.

B. Computational Complexity Analysis

The computational complexity of RGPSSM is analyzed across its various algorithmic steps in the following table, where a detailed comparison between the standard and Cholesky-based implementations of RGPSSM is presented. The analysis is based on the multi-output GP version of RGPSSM.

Table 1 Computational complexity comparison between standard and Cholesky versions of RGPSSM

Algorithm step	Standard RGPSSM	Involved equations	Cholesky RGPSSM	Involved equations
GP prediction	$\mathcal{O}((d_f M)^2)$	(10)	$\mathcal{O}((d_f M)^2)$	(10)
Moment propagation	$\mathcal{O}((d_x + d_f M)^2)$	(17), (24)	$\mathcal{O}((d_x + d_f M)^3)$	(58)-(62)
Inducing point removal	$\mathcal{O}((d_x + d_f M)^3)$	(22)	$\mathcal{O}((d_x + d_f M)^3)$	(22), (66)
Moment correction	$\mathcal{O}((d_x + d_f M)^2)$	(18)	$\mathcal{O}((d_x + d_f M)^2)$	(63)
Hyperparameter update	$\mathcal{O}((d_x + d_f M)^3)$	(31), (32)	$\mathcal{O}((d_x + d_f M)^3)$	(31), (32), (67)
Total complexity	$\mathcal{O}((d_x + d_f M)^3)$	-	$\mathcal{O}((d_x + d_f M)^3)$	-

Based on the above analysis, additional remarks regarding the computational complexity are presented below:

- By precomputing and storing the Cholesky factor of the kernel matrix \mathbf{K}_{uu} during updates, we can avoid repeated matrix inversions in GP prediction (10), thereby reducing the computational complexity to quadratic order.
- As shown in Table 1, both the standard and Cholesky versions of RGPSSM exhibit cubic total complexity. Although the Cholesky version incurs higher computational costs in certain algorithmic steps, it offers superior numerical stability. Therefore, we recommend the Cholesky version for general applications, which is adopted throughout all experimental evaluations.
- It is clear that the overall algorithmic complexity grows cubically with both the function output dimension d_f and the number of inducing points M . This is mainly due to two factors: the EKF-like moment matching, which provides second-order learning capabilities [54], and the flexible inducing point adjustment and hyperparameter optimization algorithms. Although this cubic complexity limits the algorithm's applicability to high-dimensional scenarios, it offers a stable, fast, and flexible learning solution for low-dimensional problems, which are common in many applications such as aerospace [8] and robotics [50].

C. Generalization and Applicability

RGPSSM can be regarded as a unified generalization of several existing methods. Specifically, it subsumes both the pre-parameterized AKF-based online GPSSM with inducing points [41] and kernel-based online regression approaches such as KRLS [51] and SOGP [52] as special cases. For example, if RGPSSM is initialized with a fixed set of inducing points and no further updates are performed (i.e., by setting $\varepsilon_{\text{tol}} = +\infty$), it reduces to the pre-parameterized AKF-based method. Furthermore, when the transition and measurement functions in the GPSSM are set as $x_t = f(\mathbf{c}_t)$ and $y_t = x_t$, where \mathbf{c}_t and y_t denote the function input and output, respectively, RGPSSM becomes equivalent to KRLS and SOGP. Therefore, RGPSSM offers practical and flexible recursive learning capabilities applicable to a wide range of scenarios, as summarized below:

- Applicable to several observation scenarios, including partial state observation ($y_t = g(\mathbf{x}_t)$), full state observation ($y_t = \mathbf{x}_t$), and direct function value observation ($y_t = f(\mathbf{x}_t)$).
- Benefiting from the two-step inference formulation, it is suitable for cases involving irregular measurement intervals or measurement losses.
- Since it belongs to the AKF framework, it can be seamlessly integrated with existing adaptive Kalman filtering methods to enable adaptation of process and measurement noise covariances.
- The use of first-order linearization, together with the augmentation of the inducing point set, enables a finite-dimensional Gaussian approximation of the joint state-inducing point distribution. This provides a flexible foundation for incorporating advanced nonlinear filters, such as the sigma point filter [55, 56], iterative filter [57], variational filter [58], or exact moment evaluation [59], to further improve the accuracy of moment matching.

In the next section, we will validate the effectiveness and advantages of RGPSSM through several experiments.

VI. Experiment Result

This section demonstrates the proposed method using two synthetic simulations and a real-world dataset. Section VI.A presents a comparative experiment on a synthetic NASCAR[®] dataset, which serves as a benchmark for online GPSSM methods. Section VI.B showcases the capability of RGPSSM for hyperparameter and inducing point adaptation in a synthetic wing rock dynamics learning task. Section VI.C evaluates the learning performance of RGPSSM on various real-world datasets.

The learning algorithm is implemented on a desktop computer running Python 3.9, with an Intel(R) Core(TM) i7-14700F 2.10 GHz processor and 32 GB of RAM, and the associated code is published online[‡]. In all experiments, the multi-output kernel (33) is employed, where the single-output kernel is the Squared Exponential Automatic Relevance Determination (SEARD) [15] kernel, which is defined as:

$$K_0(\mathbf{x}, \mathbf{x}') = \exp \left(-\frac{1}{2} (\mathbf{x} - \mathbf{x}')^T \mathbf{\Lambda}^{-1} (\mathbf{x} - \mathbf{x}') \right) \quad (34)$$

where the diagonal matrix $\mathbf{\Lambda} = \text{diag}(l_1^2, l_2^2, \dots, l_{d_x}^2)$ encodes the length scales for each input dimension. The signal covariance matrix $\mathbf{\Xi}$ is defined as $\text{diag}(\sigma_1^2, \sigma_2^2, \dots, \sigma_{d_f}^2)$, where each σ_i^2 denotes the signal variance corresponding to the i -th output dimension of the function. This kernel formulation enables the model to flexibly characterize both the relevance of different input features (via l_i) and the signal strength of each output (via σ_i^2). All these hyperparameters will be optimized online to adaptively capture the underlying function characteristics during learning.

A. Synthetic NASCAR[®] Dynamics Learning

To benchmark the online learning performance of RGPSSM, we compare it with two state-of-the-art algorithms: SVMC [44], which represents PF-based methods, and OEnVI [39], which exemplifies SVI-based methods. Since the pre-parameterized AKF-based method is a special case of the proposed method, it is not included in the comparison. In the experiment, all methods are tested using synthetic NASCAR[®] data [60], which involves a two-dimensional state with dynamics following a recurrent switching linear dynamical system. The measurement model is given by $\mathbf{y}_t = \mathbf{C}\mathbf{x}_t + \mathbf{w}_t$, $\mathbf{w}_t \sim N(\mathbf{0}, 0.1^2 \mathbf{I}_4)$, where $d_y = 4$ and \mathbf{C} is a 4-by-2 matrix with random elements. The three methods are trained with 500 measurements and tested by predicting the subsequent 500 steps. Note that, unlike the experiments in [44] and [39], we use fewer dimensions and a smaller number of measurements for training, providing a more rigorous evaluation. For a fair comparison, the maximum number of inducing points across all methods is limited to 20, and the GP hyperparameters are set to the same values and are not adjusted online. The implementation and other parameter

[‡]<https://github.com/TengjieZheng/rgpssm>

settings for the SVMC and OEnVI algorithms are based on the code provided online^{§ ¶}.

The experimental results are presented in Fig. 2, where the top row showcases the true and filtered state trajectories, and the bottom row depicts the filtering and prediction results. It is observed that RGPSSM and SVMC effectively extract the dynamics and provide high-accuracy predictions, while OEnVI fails to learn the dynamics due to slow convergence and the large data requirements associated with SVI. Additionally, the learning accuracy and computational efficiency are quantified in Table 2. As shown in the table, although SVMC is capable of learning system dynamics from limited measurements, it incurs a high computational cost due to the large number of particles required. In contrast, OEnVI achieves the lowest computation time but exhibits a slower learning convergence rate, primarily because it relies on a stochastic gradient optimization. However, the proposed method, grounded in the AKF framework, achieves an effective trade-off between learning convergence and computational efficiency. The EKF-like update mechanism provides second-order optimization speed [54], which is generally faster than SVI-based approaches. These results highlight the advantages and superior performance of the proposed RGPSSM method.

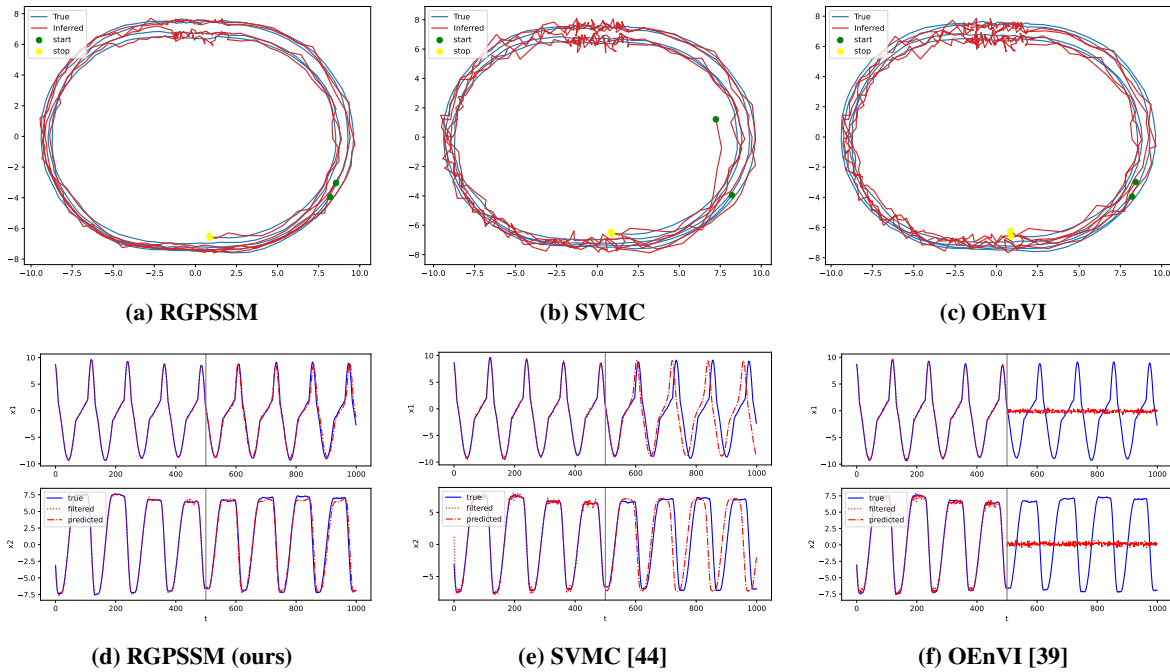


Fig. 2 Online learning results for NASCAR[®] dynamics. Top: filtered state trajectory; Bottom: filtering and prediction.

[§]<https://github.com/catnplab/svmc>

[¶]<https://github.com/zhidilin/gpssmProj>

Table 2 Prediction Accuracy and Computational Efficiency of the Three Online GPSSM Methods.

Method	RGPSSM	SVMC	OEnVI
Prediction RMSE	1.2552	5.9180	7.8583
Running Time (s)	8.59	42.69	6.55

B. Synthetic Wing Rock Dynamics Learning

To further evaluate RGPSSM's ability to online adapt GP hyperparameters and inducing points, it is tested on the synthetic wing rock dynamics learning task. In aerospace engineering, wing rock dynamics can cause roll oscillations in slender delta-winged aircraft, posing a significant threat to flight safety. To address this issue, most approaches rely on online learning of wing rock dynamics [6–8, 61]. The associated dynamical system can be expressed by the following continuous-time SSM:

$$\begin{aligned}\dot{\theta} &= p \\ \dot{p} &= L_{\delta_a} \delta_a + \Delta(\theta, p)\end{aligned}\tag{35}$$

where $\theta \in \mathbb{R}$ (deg) and $p \in \mathbb{R}$ (deg/s) denote the roll angle and roll rate, respectively. As illustrated in (35), the dynamics model consists of a known part $L_{\delta_a} \delta_a$, where δ_a is the aileron control input and $L_{\delta_a} = 3 \text{ s}^{-2}$, and an unknown uncertainty model $\Delta(\theta, p)$. The uncertainty model used in the simulation is taken from [61], namely:

$$\Delta(\theta, p) = W_0 + W_1 \theta + W_2 p + W_3 |\theta| p + W_4 |p| p + W_5 \theta^3\tag{36}$$

where $W_0 = 0.8 \text{ deg} \cdot \text{s}^{-2}$, $W_1 = 0.2314 \text{ s}^{-2}$, $W_2 = 0.6918 \text{ s}^{-1}$, $W_3 = -0.6245 \text{ deg}^{-1} \text{ s}^{-1}$, $W_4 = 0.0095 \text{ deg}^{-1}$, $W_5 = 0.0214 \text{ deg}^{-2} \text{ s}^{-2}$. To further demonstrate the learning capacity of the proposed method under sparse sensor conditions, the measurement is limited to the roll angle θ , which is corrupted by Gaussian white noise with a standard deviation of 0.2 degrees.

To apply the proposed Algorithm 1 to learn the uncertainty model $\Delta(\theta, p)$, the continuous-time dynamics (35) is discretized with time step $\Delta t = 0.05 \text{ s}$, resulting in the following transition model:

$$\mathbf{F}(\mathbf{x}_t, c_t, f(\mathbf{x}_t)) = \mathbf{x}_t + \begin{bmatrix} \mathbf{x}_t^{(2)} \\ f(\mathbf{x}_t) + L_{\delta_a} c_t \end{bmatrix} \Delta t\tag{37}$$

where the system state is defined as $\mathbf{x}_t = [\theta(t), p(t)]^\top$, with $\mathbf{x}_t^{(2)} = p(t)$, the control input $c_t = \delta_a(t)$, and the uncertainty is modeled as $f(\mathbf{x}_t) = \Delta(\theta(t), p(t))$. To enable hyperparameter adaptation, we perform one iteration of hyperparameter optimization during each RGPSSM update using a learning rate of 0.01. The number of inducing points is limited to 20. Under these settings, we evaluate the proposed method and analyze the impact of hyperparameter and

inducing point adaptation.

Firstly, we conduct a Monte Carlo test of the proposed learning algorithm with different initial values of GP hyperparameters. The simulation results are depicted in Fig. 3 and 4. As shown in Fig. 3, all three GP hyperparameters gradually converge near the reference values, which are obtained through offline GP training using data pairs (θ, p, Δ) . This indicates that the GP hyperparameters do not need to be precisely selected at the stage of algorithm initialization, and the online optimization can effectively adjust them. To evaluate the improvement resulting from hyperparameter adaptation, we calculate the prediction RMSE over the last quarter segment, which is 29.3% lower with hyperparameter adaptation than without. Furthermore, to more intuitively illustrate the benefits of hyperparameter adaptation, we present the state profile from one Monte Carlo simulation case, as shown in Fig. 4. In the figure, the blue solid lines depict the true values of state $\theta(t)$, $p(t)$ and uncertainty $\Delta(t)$; the orange dashed lines represent the filtered state and uncertainty predictions obtained without hyperparameter adaptation; and the green dashed lines show the predictions with hyperparameter adaptation. It is evident that hyperparameter adaptation improves both the mean and variance predictions of the GP, thereby enhancing the filtering accuracy of the state, especially the roll rate p . Therefore, the proposed method can not only learn the uncertain dynamics but also improve the state estimation accuracy.

Secondly, to illustrate the adaptation process of the inducing points and their advantages, we present the associated results in Fig. 5. In this figure, the inducing inputs are represented by yellow diamonds, while the true state values are shown as white circles. It is evident that the number of inducing points gradually increases to the predefined budget ($M = 20$), and the points are concentrated around the existing states. Note that the inducing points are selected from state estimation values, and therefore do not coincide with the true states. Given the localized nature of the squared exponential kernel, the selection of inducing points can effectively represent the GP model. This effectiveness is demonstrated in the background contour plot, which visualizes the distribution of prediction errors in the state space. It is evident that the prediction error decreases over time, particularly around the existing states, benefiting from the effective selection of inducing points.

C. Real-World System Identification Task

To evaluate the generalization capability of the proposed method, we conducted experiments on five real-world system identification benchmark datasets^{||}. The first half of each dataset was used for training, while the second half was reserved for testing predictive performance. Due to limited prior knowledge of the models and the restricted amount of training data, these datasets are mainly used for assessing offline GPSSM approaches. In this study, we performed an online learning experiment with the proposed method, comparing its performance against three state-of-the-art offline

^{||} <https://homes.esat.kuleuven.be/~smc/daisy/daisydata.html>

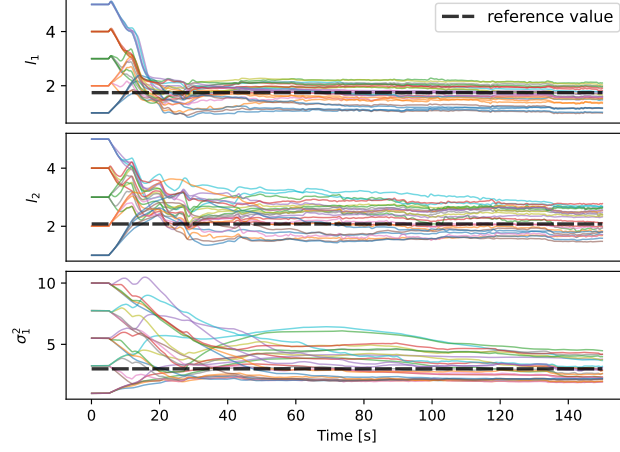


Fig. 3 Evolution of the GP hyperparameters during RGPSSM learning

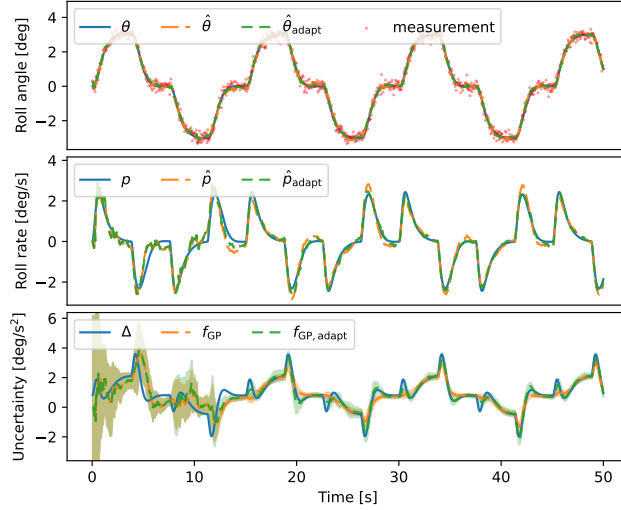


Fig. 4 Evolution of the system states and their estimation, where the initial values of the GP hyperparameters are $l_1 = l_2 = 5$ and $\sigma_1^2 = 10$. The shadows indicate 95% confidence intervals.

GPSSM techniques: PRSSM [36], VCDT [37], and EnVI [39]. For each method, the number of inducing points was capped at 20, and a 4-dimensional state GPSSM was used to capture system dynamics, with a transition model defined as $\mathbf{x}_{t+1} = f(\mathbf{x}_t, c_{t+1})$, where $\mathbf{x}_t \in \mathbb{R}^4$ and c_{t+1} is the control input, and a measurement model given by $y_t = [1, 0, 0, 0]\mathbf{x}_t$. In addition, to activate the estimation for the latent state within RGPSSM, we randomly assign an inducing point around the origin before learning to make the transition Jacobian A_x non-zero for each state dimension (see our code for details).

The experimental results from multiple simulations with different random seeds are summarized in Table 3. As shown in the table, although online learning is challenging, the proposed method achieves the best prediction accuracy on three datasets. This superior performance can be attributed to the fact that while offline methods can utilize the full dataset for repeated training, their learning accuracy is often limited by various factors, such as local optima, vanishing

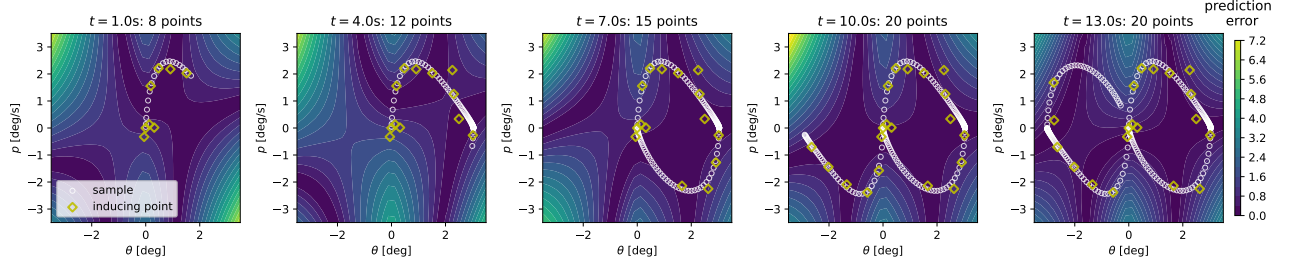


Fig. 5 Evolution of inducing-point set and prediction error over time.

or exploding gradients during SSM/RNN training [62], or insufficient expressiveness of the variational distribution (e.g., the mean-field assumption in PRSSM [36], Gaussian parametric constraints over the state and inducing points posterior in VCDT [37], or using the filtering distribution to approximate the smoothing distribution in EnVI [39]). However, RGPSSM fully considers the coupling between the system state and the GP, with only the linearization approximation limiting its learning capability. Therefore, in some cases, the online learning performance of the proposed method is comparable to that of offline methods. Of course, due to the linearization approximation, the proposed method may have limitations in highly nonlinear scenarios, which could potentially be addressed by integrating advanced nonlinear filtering techniques. Additionally, we mention that the results of online learning have the potential to provide effective initializations for offline learning, thereby improving both training speed and accuracy. This is an interesting direction that can be further explored in future work.

Table 3 Performance Comparison of Different GPSSM Methods across Five System Identification Benchmarks. Prediction RMSE is Averaged over Five Seeds, with Standard Deviations Reported in Parentheses.

Methods	Offline			Online
	PRSSM	VCDT	EnVI	RGPSSM
Actuator	0.691 (0.148)	0.815 (0.012)	0.657 (0.095)	1.048 (0.142)
Ball Beam	0.074 (0.010)	0.065 (0.005)	0.055 (0.002)	0.046 (0.002)
Drive	0.647 (0.057)	0.735 (0.005)	0.703 (0.050)	0.863 (0.083)
Dryer	0.174 (0.013)	0.667 (0.266)	0.125 (0.017)	0.105 (0.004)
Gas Furnace	1.503 (0.196)	2.052 (0.163)	1.388 (0.123)	1.373 (0.061)

VII. Conclusion

In this paper, we propose a novel recursive learning method, RGPSSM, for online inference in Gaussian Process State Space Models (GPSSMs). First, to enable learning in any operating domain, we derive a two-step Bayesian update equation that does not rely on any GP approximation, which provides a new solution for the nonlinearity and nonparametric issues of GPSSMs. Second, to mitigate the computational burden imposed by the nonparametric nature of GPs, we introduce a dynamic inducing-point set adjustment algorithm to ensure computational efficiency. Third, to eliminate the need for careful tuning of GP hyperparameters at initialization and to enhance online learning accuracy, we develop an online optimization method that extracts measurement information from the approximate posterior distribution. Fourth, we derive a Cholesky version of RGPSSM in detail to further improve numerical stability, and also present the extension of RGPSSM to the multi-output GP case. Fifth, we analyze the computational complexity of the proposed method and demonstrate that it generalizes several existing approaches, as well as highlight its strong potential for further extensions. Finally, through extensive evaluations on a diverse set of real and synthetic datasets, we demonstrate the superior learning performance and adaptability of the proposed method. In the future, research may focus on enhancing nonlinear filtering accuracy, improving computational efficiency, scaling it to high-dimensional problems, and adapting it to process and measurement noise covariances, as well as time-varying dynamics.

Appendix

A. Score for Selection of Inducing Point

This section derives the score quantifying the accuracy loss for discarding an inducing point, which is achieved based on the KL divergence in (21). As shown in (21), D_1 is unrelated to the point to discard u_d . Therefore, only D_2 and D_3 need to be evaluated. Without loss of generality, suppose the index of the discarded point u_d is $i_d = 1$.

Firstly, for D_2 , the log-term in the intergration is:

$$\begin{aligned} \log p(u_d | \mathbf{u}_1) = & -\frac{1}{2} \log(2\pi) - \frac{1}{2} \log |\gamma_d| \\ & - \frac{1}{2} (\mathbf{u}_d - \mathbf{k}_{dl} \mathbf{u}_1)^T \gamma_d^{-1} (\mathbf{u}_d - \mathbf{k}_{dl} \mathbf{u}_1) \end{aligned} \quad (38)$$

where $\mathbf{k}_{dl} = \mathbf{K}_{dl} \mathbf{K}_{ll}^{-1}$ and $\gamma_d = \mathbf{K}_{dd} - \mathbf{K}_{dl} \mathbf{K}_{ll}^{-1} \mathbf{K}_{ld}$. Denote $\mathbf{Q} = \mathbf{K}_{uu}^{-1}$, and using the matrix inversion formula (see Appendix A of [52]), we have:

$$\begin{aligned} \gamma_d &= \mathbf{Q}_{dd}^{-1} \\ \mathbf{k}_{dl} &= -\mathbf{Q}_{dd}^{-1} \mathbf{Q}_{dl} \end{aligned} \quad (39)$$

where \mathbf{Q}_{dd} denotes the i_d th diagonal element of matrix \mathbf{Q} , and \mathbf{Q}_{dl} denotes the i_d th row of \mathbf{Q} with \mathbf{Q}_{dd} removed.

Using (21), (38) and (39), the u_d relevant term in D_2 is:

$$\begin{aligned}
\tilde{D}_2 &= \frac{1}{2} \log |\mathbf{Q}_{dd}| - \frac{1}{2} \Delta \\
\Delta &= \int q(\mathbf{u}) (\mathbf{u}_d - \mathbf{k}_{dl} \mathbf{u}_1)^T \mathbf{Q}_{dd} (\mathbf{u}_d - \mathbf{k}_{dl} \mathbf{u}_1) d\mathbf{u} \\
&= \mathbb{E}_{q(\mathbf{u})} \left[\text{tr} \left(\mathbf{Q}_{dd} (\mathbf{u}_d - \mathbf{k}_{dl} \mathbf{u}_1) (\mathbf{u}_d - \mathbf{k}_{dl} \mathbf{u}_1)^T \right) \right] \\
&= \text{tr} \left(\mathbf{Q}_{dd} \mathbb{E}_{q(\mathbf{u})} \left[(\mathbf{u}_d - \mathbf{k}_{dl} \mathbf{u}_1) (\mathbf{u}_d - \mathbf{k}_{dl} \mathbf{u}_1)^T \right] \right)
\end{aligned} \tag{40}$$

Let $\boldsymbol{\phi} = [1, -\mathbf{k}_{dl}]$, and then we have $\mathbf{u}_d - \mathbf{k}_{dl} \mathbf{u}_1 = \boldsymbol{\phi} \mathbf{u}$. Using (39), we further have:

$$\begin{aligned}
\boldsymbol{\phi} &= \begin{bmatrix} 1 & \mathbf{Q}_{dd}^{-1} \mathbf{Q}_{dl} \end{bmatrix} \\
&= \begin{bmatrix} \mathbf{Q}_{dd}^{-1} \mathbf{Q}_{dd} & \mathbf{Q}_{dd}^{-1} \mathbf{Q}_{dl} \end{bmatrix} \\
&= \mathbf{Q}_{dd}^{-1} \mathbf{Q}_{du}
\end{aligned} \tag{41}$$

where \mathbf{Q}_{du} denotes the i_d th row of \mathbf{Q} . Therefore:

$$\begin{aligned}
\Delta &= \text{tr} \left(\mathbf{Q}_{dd} \mathbb{E}_{q(\mathbf{u})} \left[\boldsymbol{\phi} \mathbf{u} \mathbf{u}^T \boldsymbol{\phi}^T \right] \right) \\
&= \text{tr} \left(\mathbf{Q}_{dd} \left[\boldsymbol{\phi} (S_{uu} + \mathbf{m}_u \mathbf{m}_u^T) \boldsymbol{\phi}^T \right] \right) \\
&= \Delta_1 + \Delta_2
\end{aligned} \tag{42}$$

where

$$\begin{aligned}
\Delta_1 &= \mathbf{m}_u^T \mathbf{Q}_{du}^T \mathbf{Q}_{dd}^{-1} \mathbf{Q}_{du} \mathbf{m}_u \\
\Delta_2 &= \text{tr} \left(\mathbf{Q}_{du} S_{uu} \mathbf{Q}_{du}^T \mathbf{Q}_{dd}^{-1} \right)
\end{aligned} \tag{43}$$

For D_3 , we can use the differential entropy identical for Gaussian distribution:

$$\int p(\mathbf{a}) \log p(\mathbf{a}) d\mathbf{a} = -\frac{1}{2} [n_a + n_a \log(2\pi) + \log |\boldsymbol{\Sigma}_a|] \tag{44}$$

where $p(\mathbf{a})$ is a n_a -dimension Gaussian distribution with covariance $\boldsymbol{\Sigma}_a$. Deonte the covariance of joint distribution $q(\mathbf{X}_t)$ that marginal out \mathbf{u}_d as $\boldsymbol{\Sigma}_{t,l}$, and deonte the inversion of original covariance as $\boldsymbol{\Omega} = \boldsymbol{\Sigma}_t^{-1}$. Then, given (44), the \mathbf{u}_d relevant term in D_3 is:

$$\begin{aligned}
-\frac{1}{2} \log |\boldsymbol{\Sigma}_{t,l}| &= -\frac{1}{2} \log \left(|\boldsymbol{\Sigma}_t| / |S_{dd} - \boldsymbol{\zeta}_d^T \boldsymbol{\Sigma}_{t,l} \boldsymbol{\zeta}_d| \right) \\
&= -\frac{1}{2} \log |\boldsymbol{\Sigma}_t| - \frac{1}{2} \log |\boldsymbol{\Omega}_{dd}| \\
\boldsymbol{\zeta}_d &= \begin{bmatrix} \mathbf{V}_{xd} \\ S_{ud} \end{bmatrix}
\end{aligned} \tag{45}$$

where $\mathbf{\Omega}_{dd}$ is the element of the matrix $\mathbf{\Omega}$ corresponding to the discarded point u_d , namely, its $(d_x + i_d)$ -th diagonal element. In addition, (45) is derived by using the properties of the determinants of block matrices and the matrix inversion formula (see Appendix A of [52]).

Based on the KL divergence (21) and combining (40), (43) and (45), we have the score:

$$s_d = \Delta_1 + \Delta_2 + \Delta_3 \quad (46)$$

where

$$\Delta_3 = \log |\mathbf{\Omega}_{dd}| - \log |\mathbf{Q}_{dd}| \quad (47)$$

In terms of effect, a lower value of the score s_d implies less accuracy loss for discarding the point u_d .

B. Prediction Equation without Adding Points

According to (20), if the new inducing point f_t is discarded in the prediction step, the distribution after discarding can be given by:

$$\hat{q}^*(\mathbf{x}_{t+1}, \mathbf{u}) = \int q^-(\mathbf{x}_{t+1}, \bar{\mathbf{u}}) d\bar{f}_t \quad (48)$$

Then, by incorporating the original prediction equation (14), we have:

$$\begin{aligned} \hat{q}^*(\mathbf{x}_{t+1}, \mathbf{u}) &= \int \int q(\mathbf{x}_{t+1} | \mathbf{x}_t, f_t) q(\mathbf{x}_t, \bar{\mathbf{u}}) d\mathbf{x}_t d\bar{f}_t \\ &= \int \int q(\mathbf{x}_{t+1} | \mathbf{x}_t, f_t) p(f_t | \mathbf{u}) q(\mathbf{x}_t, \mathbf{u}) d\mathbf{x}_t df_t \\ &= \int q(\mathbf{x}_{t+1} | \mathbf{x}_t, \mathbf{u}) q(\mathbf{x}_t, \mathbf{u}) d\mathbf{x}_t \end{aligned} \quad (49)$$

where $q(\mathbf{x}_{t+1} | \mathbf{x}_t, \mathbf{u})$ represents a new transition model, whose specific expression is:

$$\begin{aligned} q(\mathbf{x}_{t+1} | \mathbf{x}_t, \mathbf{u}) &= \int q(\mathbf{x}_{t+1} | \mathbf{x}_t, f_t) p(f_t | \mathbf{u}) df_t \\ &= \int q(\mathbf{x}_{t+1} | \mathbf{x}_t, f_t) \mathcal{N}(f_t | \mathbf{k}_{tu}\mathbf{u}, \gamma) df_t \\ &= \mathcal{N}\left(\mathbf{x}_{t+1} \middle| \mathbf{F}_t + \mathbf{A}_x(\mathbf{x}_t - \boldsymbol{\mu}_t) + \mathbf{A}_f \mathbf{k}_{tu}(\mathbf{u} - \mathbf{m}_u), \tilde{\boldsymbol{\Sigma}}_f\right) \end{aligned} \quad (50)$$

where $\gamma = \mathbf{K}_{tt} - \mathbf{K}_{tu}\mathbf{K}_{uu}^{-1}\mathbf{K}_{ut}$ and $\tilde{\boldsymbol{\Sigma}}_f = \mathbf{A}_f\gamma\mathbf{A}_f^T + \boldsymbol{\Sigma}_p$.

Combining (49) and (50), the prediction equation (24) can be obtained.

C. Derivation Details of GP Hyperparameters Optimization

This section derives the moments of the approximate joint distribution $q_{new}(\mathbf{x}_t, \mathbf{f})$ in (29), along with the optimizing objective for GP hyperparameters.

Firstly, to derive the moments of the approximate joint distribution $q_{new}(\mathbf{x}_t, \mathbf{f})$, we can utilize the following result:

$$\begin{aligned} \frac{p(\mathbf{u}; \boldsymbol{\theta}_{new})}{p(\mathbf{u}; \boldsymbol{\theta}_{old})} &= \frac{\mathcal{N}(\mathbf{u} | \mathbf{0}, \mathbf{K}_{uu}^{new})}{\mathcal{N}(\mathbf{u} | \mathbf{0}, \mathbf{K}_{uu}^{old})} \\ &= Z \mathcal{N}(\mathbf{u} | \mathbf{0}, \Delta \mathbf{K}) \\ &= Z \mathcal{N}(\mathbf{0} | \mathbf{u}, \Delta \mathbf{K}) \end{aligned} \quad (51)$$

where

$$\begin{aligned} \Delta \mathbf{K} &= [(\mathbf{K}_{uu}^{new})^{-1} - (\mathbf{K}_{uu}^{old})^{-1}]^{-1} \\ Z &\propto \frac{|\mathbf{K}_{uu}^{old}|^{1/2} |\Delta \mathbf{K}|^{1/2}}{|\mathbf{K}_{uu}^{new}|^{1/2}} \end{aligned} \quad (52)$$

Note that, the above equations hold only in a mathematical sense and does not have probabilistic meaning, as $\Delta \mathbf{K}$ may not be positive definite. Combining (29) and (51), we have:

$$q_{new}(\mathbf{x}_t, \mathbf{u}) \propto \mathcal{N}(\mathbf{0} | \mathbf{u}, \Delta \mathbf{K}) q_{old}(\mathbf{x}_t, \mathbf{u}) \quad (53)$$

whose moments can be obtained by the correction equation of Kalman filter:

$$\begin{aligned} \tilde{\mathbf{H}} &= \begin{bmatrix} \mathbf{0} & \mathbf{I}_{n_u} \end{bmatrix} \\ \tilde{\mathbf{G}} &= \boldsymbol{\Sigma}_t^{old} \tilde{\mathbf{H}}^T (\mathbf{S}_{uu}^{old} + \Delta \mathbf{K})^{-1} \\ \boldsymbol{\xi}_t^{new} &= \boldsymbol{\xi}_t^{old} - \tilde{\mathbf{G}} \boldsymbol{\xi}_t^{old} \\ \boldsymbol{\Sigma}_t^{new} &= \boldsymbol{\Sigma}_t^{old} - \tilde{\mathbf{G}} \tilde{\mathbf{H}} \boldsymbol{\Sigma}_t^{old} \end{aligned} \quad (54)$$

where $\boldsymbol{\xi}_t$ and $\boldsymbol{\Sigma}_t$ represents the mean and covariance of the augmented state $\mathbf{X}_t = [\mathbf{x}_t^T, \mathbf{u}^T]^T$.

Secondly, in order to optimize the GP hyperparameters, considering (30) and (51), we can maximize:

$$\begin{aligned} &\log \frac{p(\mathbf{y}_{1:t}; \boldsymbol{\theta}_{new})}{p(\mathbf{y}_{1:t}; \boldsymbol{\theta}_{old})} \\ &= \log \int Z \mathcal{N}(\mathbf{0} | \mathbf{u}, \Delta \mathbf{K}) q_{old}(\mathbf{x}_t, \mathbf{u}) d\mathbf{x}_t d\mathbf{u} \\ &= \log \mathcal{N}(\mathbf{0} | \mathbf{m}_u^{old}, \Delta \mathbf{K} + \mathbf{S}_{uu}^{old}) + \log Z \end{aligned} \quad (55)$$

Then, by dropping some $\boldsymbol{\theta}_{new}$ -irrelevant terms, the optimization objective can be transformed to minimize:

$$\mathcal{L} = \mathcal{L}_1 + \mathcal{L}_2 \quad (56)$$

where

$$\begin{aligned} \mathcal{L}_1 &= (\mathbf{m}_u^{old})^T (\mathbf{S}_{uu}^{old} + \Delta \mathbf{K})^{-1} \mathbf{m}_u^{old} \\ \mathcal{L}_2 &= -\log |\Delta \mathbf{K}| + \log |\mathbf{K}_{uu}^{new}| + \log |\Delta \mathbf{K} + \mathbf{S}_{uu}^{old}| \\ &= \log |\mathbf{K}_{uu}^{new}| + \log |\mathbf{I}_{n_u} + \Delta \mathbf{K}^{-1} \mathbf{S}_{uu}^{old}| \\ &= \log |\mathbf{K}_{uu}^{new}| + [\mathbf{I}_{n_u} - \mathbf{K}_{uu}^{new} (\mathbf{K}_{uu}^{old})^{-1}] \mathbf{S}_{uu}^{old} | \end{aligned} \quad (57)$$

Here, we avoid the appearance of $\Delta \mathbf{K}$ in the loss function through some operations, because when $\mathbf{K}_{uu}^{new} = \mathbf{K}_{uu}^{old}$, $\Delta \mathbf{K}$ is not well-defined.

D. Stable Implementation Method

To solve the numerical stability problem in RGPSSM, this section develops a stable implementation method based on Cholesky decomposition. Specifically, the covariance Σ_t of the augmented state \mathbf{X}_t is decomposed as $\Sigma_t = \mathbf{L}_t \mathbf{L}_t^T$, where \mathbf{L}_t is a lower triangular matrix, known as the Cholesky factor. Based on this decomposition, the evolution of the covariance Σ_t is replaced by the evolution of the Cholesky factor, which can reduce the accumulation of computational rounding errors. To implement this method, we must modify the moment matching equations within the prediction and correction steps, as well as during the discarding of inducing points and hyperparameter optimization.

For the prediction step, there exist two cases: not adding points and adding points. Firstly, for the prediction equation without adding points (24), the covariance update can be rewritten by:

$$\Sigma_{t+1}^- = \begin{bmatrix} \Phi_t \mathbf{L}_t & \mathbf{D}_f \end{bmatrix} \begin{bmatrix} \mathbf{L}_t^T \Phi_t^T \\ \mathbf{D}_f^T \end{bmatrix} \quad (58)$$

where \mathbf{D}_f is the Cholesky factor of the process noise covariance $\Sigma_{p,X}$. Then, through the following QR decomposition:

$$\begin{bmatrix} \mathbf{L}_t^T \Phi_t^T \\ \mathbf{D}_f^T \end{bmatrix} = \mathbf{O} \mathbf{R} \quad (59)$$

where \mathbf{O} is an orthogonal matrix and \mathbf{R} is an upper triangular matrix, we can obtain the Cholesky factor of the predicted covariance Σ_{t+1}^- , namely, $\mathbf{L}_{t+1}^- = \mathbf{R}^T$.

Then, for the case of prediction with adding points, it involves one additional step: evaluating the Cholesky factor $\bar{\mathbf{L}}_t$ of the augmented covariance $\bar{\Sigma}_t$ after adding a point. According to the definition, the augmented covariance $\bar{\Sigma}_t$ can

be expressed as follows:

$$\bar{\Sigma}_t = \begin{bmatrix} \Sigma_t & \zeta_t \\ \zeta_t^T & S_{tt} \end{bmatrix}, \quad \zeta_t = \begin{bmatrix} V_{xt} \\ S_{ut} \end{bmatrix} \quad (60)$$

In view of this expression, we can define:

$$\bar{L}_t = \begin{bmatrix} L_t & \mathbf{0} \\ \alpha & \beta \end{bmatrix} \quad (61)$$

and correspondingly we have:

$$\bar{\Sigma}_t = \begin{bmatrix} L_t L_t^T & L_t \alpha^T \\ \alpha^T L_t^T & \alpha \alpha^T + \beta \beta^T \end{bmatrix} \quad (62)$$

Combining (60) and (62), we can obtain α by solving the linear equation $L_t \alpha^T = \zeta_t$, and then compute $\beta = \text{cholesky}(S_{tt} - \alpha \alpha^T)$, thus obtaining the Cholesky factor \bar{L}_t . Then, similar operations as in (58) and (59) can be implemented to evaluate the predicted Cholesky factor.

For the correction step, given (18), the update equation for covariance can be rewritten as:

$$\begin{aligned} \Sigma_{t+1} &= \Sigma_{t+1}^- - \Sigma_{t+1}^- H^T (C P_{t+1}^- C^T + \Sigma_m)^{-1} H \Sigma_{t+1}^- \\ &= \Sigma_{t+1}^- - \Sigma_{t+1}^- H^T (\rho \rho^T)^{-1} H \Sigma_{t+1}^- \\ &= L_{t+1}^- L_{t+1}^{-T} - \eta \eta^T \end{aligned} \quad (63)$$

where $\rho = \text{cholesky}(C P_{t+1}^- C^T + \Sigma_m)$ and $\eta = \Sigma_{t+1}^- H^T (\rho^{-1})^T$. According to (63), we can compute the Cholesky factor L_{t+1} of the posterior covariance Σ_{t+1} using the Cholesky downdate algorithm (see Section 6.5.4 of [63]), that is, $L_{t+1} = \text{choldowndate}(L_{t+1}^-, \eta)$. The downdate algorithm is more efficient, with quadratic complexity compared to the cubic complexity of direct decomposition.

For discarding an inducing point, to evaluate the updated Cholesky factor, we can express the original Cholesky factor before discarding as follows:

$$L_t = \begin{bmatrix} A & \mathbf{0} & \mathbf{0} \\ a & b & \mathbf{0} \\ B & c & C \end{bmatrix} \quad (64)$$

Here, we reuse the notation A, B, C, a, b, c , where a, b, c denote the blocks corresponding to the discarded point u_d .

Given (20), the updated covariance Σ'_t is the original one with the i_d th row and i_d th column removed, which can be given using the expression in (64):

$$\Sigma'_t = \begin{bmatrix} AA^T & AB^T \\ BA^T & BB^T + cc^T + CC^T \end{bmatrix} \quad (65)$$

In view of this expression, the updated Cholesky factor L'_t can be given by:

$$L'_t = \begin{bmatrix} A & \mathbf{0} \\ B & \text{cholupdate}(C, c) \end{bmatrix} \quad (66)$$

where $\text{cholupdate}(\cdot, \cdot)$ denotes the Cholesky update algorithm (see Section 6.5.4 of [63]), namely a efficient method for evaluating the Cholesky factor of $(cc^T + CC^T)$.

For hyperparameter optimization, since ΔK in (32) may not be positive definite as illustrated in Appendix VII.C, we cannot update the Cholesky factor as in the correction step. Therefore, the updated Cholesky factor is evaluated by directly decomposing the updated covariance Σ_t^{new} , which is obtained using (32):

$$L_t^{\text{new}} = \text{cholesky}(\Sigma_t^{\text{new}}) \quad (67)$$

Overall, the Cholesky versions of the update equations in the prediction and correction steps, as well as for discarding inducing points and optimizing hyperparameters, have been derived, which makes the computations more compact, thereby enhancing numerical stability.

References

- [1] Qu, D., Wang, Q., and Liu, H., “Physics-Informed Transfer Learning-Based Aerodynamic Parameter Identification of Morphing Aircraft,” *Journal of Guidance, Control, and Dynamics*, Vol. 48, No. 2, 2025, pp. 240–254. doi:10.2514/1.G008503.
- [2] Qu, C., Cheng, L., Gong, S., and Huang, X., “Experience Replay Enhances Excitation Condition of Neural-Network Adaptive Control Learning,” *Journal of Guidance, Control and Dynamics*, Vol. 48, No. 3, 2025, pp. 496–507. doi:10.2514/1.G008162.
- [3] Hua, B., Yang, G., Wu, Y., and Chen, Z., “Space Extended Target Tracking Using Poisson Multi-Bernoulli Mixture Filtering with Nonlinear Measurements,” *Journal of Guidance, Control, and Dynamics*, Vol. 47, No. 1, 2024, pp. 87–98. doi:10.2514/1.G007569.
- [4] Sun, Z., Garcia de Marina, H., Anderson, B. D., and Yu, C., “Collaborative target-tracking control using multiple fixed-wing unmanned aerial vehicles with constant speeds,” *Journal of Guidance, Control, and Dynamics*, Vol. 44, No. 2, 2021, pp. 238–250. doi:10.2514/1.G005092.

- [5] Goel, A., and Bernstein, D. S., “Injection-Constrained State Estimation,” *Journal of Guidance, Control, and Dynamics*, Vol. 45, No. 6, 2022, pp. 990–1001. doi:10.2514/1.G006108.
- [6] Lee, K. W., and Singh, S. N., “Noncertainty-equivalent adaptive wing-rock control via Chebyshev neural network,” *Journal of Guidance, Control, and Dynamics*, Vol. 37, No. 1, 2014, pp. 123–133. doi:10.2514/1.61639.
- [7] Li, D., Tsourdos, A., Wang, Z., and Ignatyev, D., “Nonlinear analysis for wing-rock system with adaptive control,” *Journal of Guidance, Control, and Dynamics*, Vol. 45, No. 11, 2022, pp. 2174–2181. doi:10.2514/1.G006775.
- [8] Singh, S. N., Yirn, W., and Wells, W. R., “Direct adaptive and neural control of wing-rock motion of slender delta wings,” *Journal of Guidance, control, and Dynamics*, Vol. 18, No. 1, 1995, pp. 25–30. doi:10.2514/3.56652.
- [9] Scampicchio, A., Arcari, E., Lahr, A., and Zeilinger, M. N., “Gaussian processes for dynamics learning in model predictive control,” *arXiv preprint arXiv:2502.02310*, 2025. doi:10.48550/arXiv.2502.02310.
- [10] Rangapuram, S. S., Seeger, M. W., Gasthaus, J., Stella, L., Wang, Y., and Januschowski, T., “Deep state space models for time series forecasting,” *Advances in neural information processing systems*, Vol. 31, 2018. URL <https://proceedings.neurips.cc/paper/2018/hash/5cf68969fb67aa6082363a6d4e6468e2-Abstract.html>.
- [11] Gedon, D., Wahlström, N., Schön, T. B., and Ljung, L., “Deep state space models for nonlinear system identification,” *IFAC-PapersOnLine*, Vol. 54, No. 7, 2021, pp. 481–486. doi:10.48550/arXiv.2003.14162.
- [12] Frigola-Alcalde, R., “Bayesian time series learning with Gaussian processes,” Ph.d. thesis, University of Cambridge, Cambridge, UK, Aug. 2015. doi:10.17863/CAM.46480.
- [13] Zheng, T., Cheng, L., Gong, S., and Huang, X., “Model Incremental Learning of Flight Dynamics Enhanced by Sample Management,” *Aerospace Science and Technology*, 2025, p. 110049. doi:10.1016/j.ast.2025.110049.
- [14] Turner, R., Deisenroth, M., and Rasmussen, C., “State-space inference and learning with Gaussian processes,” *Proceedings of the thirteenth international conference on artificial intelligence and statistics*, JMLR Workshop and Conference Proceedings, 2010, pp. 868–875. URL <https://proceedings.mlr.press/v9/turner10a.html>.
- [15] Rasmussen, C. E., and Williams, C. K. I., *Gaussian Processes for Machine Learning*, MIT Press, Cambridge, MA, USA, 2006, Chap. 2. URL <http://www.gaussianprocess.org/gpml/>.
- [16] Carè, A., Carli, R., Dalla Libera, A., Romeres, D., and Pillonetto, G., “Kernel methods and gaussian processes for system identification and control: A road map on regularized kernel-based learning for control,” *IEEE Control Systems Magazine*, Vol. 43, No. 5, 2023, pp. 69–110. doi:10.1109/MCS.2023.3291625.
- [17] Titsias, M., “Variational learning of inducing variables in sparse Gaussian processes,” *Artificial intelligence and statistics*, PMLR, 2009, pp. 567–574. URL <https://proceedings.mlr.press/v5/titsias09a.html>.
- [18] Bui, T. D., Yan, J., and Turner, R. E., “A unifying framework for Gaussian process pseudo-point approximations using power expectation propagation,” *Journal of Machine Learning Research*, Vol. 18, No. 104, 2017, pp. 1–72. doi:10.17863/CAM.20846.

- [19] Lázaro-Gredilla, M., Quinonero-Candela, J., Rasmussen, C. E., and Figueiras-Vidal, A. R., “Sparse spectrum Gaussian process regression,” *The Journal of Machine Learning Research*, Vol. 11, 2010, pp. 1865–1881. doi:doi:10.1007/s10846-009-9348-4.
- [20] Solin, A., and Särkkä, S., “Hilbert space methods for reduced-rank Gaussian process regression,” *Statistics and Computing*, Vol. 30, No. 2, 2020, pp. 419–446. doi:10.1007/s11222-019-09886-w.
- [21] Sauer, A., Cooper, A., and Gramacy, R. B., “Vecchia-approximated deep Gaussian processes for computer experiments,” *Journal of Computational and Graphical Statistics*, Vol. 32, No. 3, 2023, pp. 824–837. doi:10.1080/10618600.2022.2129662.
- [22] Wu, L., Pleiss, G., and Cunningham, J. P., “Variational nearest neighbor Gaussian process,” *International Conference on Machine Learning*, PMLR, 2022, pp. 24114–24130. URL <https://proceedings.mlr.press/v162/wu22h.html>.
- [23] Lin, J. A., Ament, S., Balandat, M., Eriksson, D., Hernández-Lobato, J. M., and Bakshy, E., “Scalable Gaussian Processes with Latent Kronecker Structure,” *arXiv preprint arXiv:2506.06895*, 2025. doi:10.48550/arXiv.2506.06895.
- [24] Damianou, A., and Lawrence, N. D., “Deep gaussian processes,” *Artificial intelligence and statistics*, PMLR, 2013, pp. 207–215. URL <https://proceedings.mlr.press/v31/damianou13a.html>.
- [25] Dong, W., and Sun, S., “Multi-view deep Gaussian processes for supervised learning,” *IEEE Transactions on Pattern Analysis and Machine Intelligence*, Vol. 45, No. 12, 2023, pp. 15137–15153. doi:10.1109/TPAMI.2023.3316671.
- [26] Lu, Q., Karanikolas, G. V., and Giannakis, G. B., “Incremental ensemble Gaussian processes,” *IEEE Transactions on Pattern Analysis and Machine Intelligence*, Vol. 45, No. 2, 2022, pp. 1876–1893. doi:10.1109/TPAMI.2022.3157197.
- [27] Csató, L., and Oppér, M., “Sparse on-line Gaussian processes,” *Neural computation*, Vol. 14, No. 3, 2002, pp. 641–668. doi:10.1162/089976602317250933.
- [28] Nguyen-Tuong, D., Peters, J., and Seeger, M., “Local Gaussian process regression for real time online model learning,” *Advances in neural information processing systems*, Vol. 21, 2008. URL <https://proceedings.neurips.cc/paper/2008/hash/01161aaa0b6d1345dd8fe4e481144d84-Abstract.html>.
- [29] Bui, T. D., Nguyen, C., and Turner, R. E., “Streaming sparse Gaussian process approximations,” *Advances in Neural Information Processing Systems*, Vol. 30, 2017. doi:10.48550/arXiv.1705.07131.
- [30] Fisac, J. F., Akametalu, A. K., Zeilinger, M. N., Kaynama, S., Gillula, J., and Tomlin, C. J., “A general safety framework for learning-based control in uncertain robotic systems,” *IEEE Transactions on Automatic Control*, Vol. 64, No. 7, 2018, pp. 2737–2752.
- [31] Frigola, R., Lindsten, F., Schön, T. B., and Rasmussen, C. E., “Bayesian inference and learning in Gaussian process state-space models with particle MCMC,” *Advances in neural information processing systems*, Vol. 26, 2013. doi:10.9774/GLEAF.978-1-909493-38-4_2.
- [32] Frigola, R., Chen, Y., and Rasmussen, C. E., “Variational Gaussian process state-space models,” *Advances in neural information processing systems*, Vol. 27, 2014. doi:10.48550/arXiv.1406.4905.

- [33] Svensson, A., and Schön, T. B., “A flexible state–space model for learning nonlinear dynamical systems,” *Automatica*, Vol. 80, 2017, pp. 189–199. doi:10.1016/j.automatica.2017.02.030.
- [34] Fan, X., Bonilla, E. V., O’Kane, T., and Sisson, S. A., “Free-form variational inference for Gaussian process state-space models,” *International Conference on Machine Learning*, PMLR, 2023, pp. 9603–9622. URL <https://proceedings.mlr.press/v202/fan23a.html>.
- [35] Eleftheriadis, S., Nicholson, T., Deisenroth, M., and Hensman, J., “Identification of Gaussian process state space models,” *Advances in neural information processing systems*, Vol. 30, 2017. doi:10.48550/arXiv.1705.10888.
- [36] Doerr, A., Daniel, C., Schiegg, M., Duy, N.-T., Schaal, S., Toussaint, M., and Sebastian, T., “Probabilistic recurrent state-space models,” *International conference on machine learning*, PMLR, 2018, pp. 1280–1289. doi:10.48550/arXiv.1801.10395.
- [37] Ialongo, A. D., Van Der Wilk, M., Hensman, J., and Rasmussen, C. E., “Overcoming mean-field approximations in recurrent Gaussian process models,” *International Conference on Machine Learning*, PMLR, 2019, pp. 2931–2940. doi:10.48550/arXiv.1906.05828.
- [38] Lindinger, J., Rakitsch, B., and Lippert, C., “Laplace approximated Gaussian process state-space models,” *Uncertainty in Artificial Intelligence*, PMLR, 2022, pp. 1199–1209. URL <https://proceedings.mlr.press/v180/lindinger22a.html>.
- [39] Lin, Z., Sun, Y., Yin, F., and Thiéry, A. H., “Ensemble Kalman filtering meets Gaussian process SSM for non-mean-field and online inference,” *IEEE Transactions on Signal Processing*, 2024. doi:10.1109/TSP.2024.3448291.
- [40] Veibäck, C., Olofsson, J., Lauknes, T. R., and Hendeby, G., “Learning target dynamics while tracking using Gaussian processes,” *IEEE Transactions on Aerospace and Electronic Systems*, Vol. 56, No. 4, 2019, pp. 2591–2602. doi:10.1109/TAES.2019.2948699.
- [41] Kullberg, A., Skog, I., and Hendeby, G., “Learning driver behaviors using a Gaussian process augmented state-space model,” *2020 IEEE 23rd International Conference on Information Fusion (FUSION)*, IEEE, 2020, pp. 1–7. doi:10.23919/FUSION45008.2020.9190245.
- [42] Kullberg, A., “On Joint State Estimation and Model Learning Using Gaussian Process Approximations,” Ph.D. thesis, Linköping University Electronic Press, 2021. doi:10.3384/9789179291426.
- [43] Berntorp, K., “Online Bayesian inference and learning of Gaussian-process state–space models,” *Automatica*, Vol. 129, 2021, p. 109613. doi:10.1016/j.automatica.2021.109613.
- [44] Zhao, Y., Nassar, J., Jordan, I., Bugallo, M., and Park, I. M., “Streaming variational monte carlo,” *IEEE transactions on pattern analysis and machine intelligence*, Vol. 45, No. 1, 2022, pp. 1150–1161. doi:10.1109/TPAMI.2022.3153225.
- [45] Liu, Y., Ajirak, M., and Djurić, P. M., “Sequential estimation of Gaussian process-based deep state-space models,” *IEEE Transactions on Signal Processing*, 2023. doi:10.1109/TSP.2023.3303648.
- [46] Grisetti, G., Stachniss, C., and Burgard, W., “Improved techniques for grid mapping with rao-blackwellized particle filters,” *IEEE transactions on Robotics*, Vol. 23, No. 1, 2007, pp. 34–46. doi:10.1109/TRO.2006.889486.

- [47] Doucet, A., Johansen, A. M., et al., “A tutorial on particle filtering and smoothing: Fifteen years later,” *Handbook of nonlinear filtering*, Vol. 12, No. 656-704, 2009, p. 3. doi:10.1109/TAC.2018.2876389.
- [48] Park, S.-S., Park, Y.-J., Min, Y., and Choi, H.-L., “Online Gaussian process state-space model: Learning and planning for partially observable dynamical systems,” *International Journal of Control, Automation and Systems*, Vol. 20, No. 2, 2022, pp. 601–617. doi:10.1007/s12555-020-0538-y.
- [49] Ljung, L., “Asymptotic behavior of the extended Kalman filter as a parameter estimator for linear systems,” *IEEE Transactions on Automatic Control*, Vol. 24, No. 1, 2003, pp. 36–50. doi:10.1109/TAC.1979.1101943.
- [50] O’Connell, M., Shi, G., Shi, X., Azizzadenesheli, K., Anandkumar, A., Yue, Y., and Chung, S.-J., “Neural-fly enables rapid learning for agile flight in strong winds,” *Science Robotics*, Vol. 7, No. 66, 2022, p. eabm6597. doi:10.48550/arXiv.2205.06908.
- [51] Van Vaerenbergh, S., Lázaro-Gredilla, M., and Santamaría, I., “Kernel recursive least-squares tracker for time-varying regression,” *IEEE transactions on neural networks and learning systems*, Vol. 23, No. 8, 2012, pp. 1313–1326. doi:10.1109/TNNLS.2012.2200500.
- [52] Csató, L., “Gaussian processes: iterative sparse approximations,” Ph.D. thesis, Aston University, Birmingham, UK, March 2002. doi:10.1080/02664763.2011.559374.
- [53] Kingma, D. P., “Adam: A method for stochastic optimization,” *arXiv preprint arXiv:1412.6980*, 2014. doi:10.48550/arXiv.1412.6980.
- [54] Eon Bottou, L., “Online learning and stochastic approximations,” *Online learning in neural networks*, Vol. 17, No. 9, 1998, p. 142. URL https://wiki.eecs.yorku.ca/course_archive/2012-13/F/6328/_media/bottou-onlinelearning-98.pdf.
- [55] Wan, E. A., and Van Der Merwe, R., “The unscented Kalman filter for nonlinear estimation,” *Proceedings of the IEEE 2000 adaptive systems for signal processing, communications, and control symposium (Cat. No. 00EX373)*, Ieee, 2000, pp. 153–158. doi:10.1109/ASSPCC.2000.882463.
- [56] Arasaratnam, I., and Haykin, S., “Cubature kalman filters,” *IEEE Transactions on automatic control*, Vol. 54, No. 6, 2009, pp. 1254–1269. doi:10.1109/TAC.2009.2019800.
- [57] Kullberg, A., Skoglund, M. A., Skog, I., and Hendeby, G., “Dynamically Iterated Filters: A unified framework for improved iterated filtering and smoothing,” *arXiv preprint arXiv:2404.15359*, 2024. doi:10.48550/arXiv.2404.15359.
- [58] Dowling, M., Zhao, Y., and Park, M., “eXponential FAMily dynamical systems (XFADS): Large-scale nonlinear gaussian state-space modeling,” *Advances in Neural Information Processing Systems*, Vol. 37, 2024, pp. 13458–13488. URL https://proceedings.neurips.cc/paper_files/paper/2024/hash/18595bc3e802a3b11035927fd928eb9c-Abstract-Conference.html.

- [59] Deisenroth, M. P., Huber, M. F., and Hanebeck, U. D., “Analytic moment-based Gaussian process filtering,” *Proceedings of the 26th annual international conference on machine learning*, 2009, pp. 225–232. doi:10.1145/1553374.1553403.
- [60] Linderman, S., Johnson, M., Miller, A., Adams, R., Blei, D., and Paninski, L., “Bayesian learning and inference in recurrent switching linear dynamical systems,” *Artificial intelligence and statistics*, PMLR, 2017, pp. 914–922. URL <https://proceedings.mlr.press/v54/linderman17a.html>.
- [61] Chowdhary, G., Kingravi, H. A., How, J. P., and Vela, P. A., “Bayesian nonparametric adaptive control using Gaussian processes,” *IEEE transactions on neural networks and learning systems*, Vol. 26, No. 3, 2014, pp. 537–550. doi:10.1109/TNNLS.2014.2319052.
- [62] Pascanu, R., Mikolov, T., and Bengio, Y., “On the difficulty of training recurrent neural networks,” *International conference on machine learning*, Pmlr, 2013, pp. 1310–1318. doi:10.1007/s12088-011-0245-8.
- [63] Golub, G. H., and Loan, C. F. V., *Matrix Computations*, 4th ed., Johns Hopkins Studies in the Mathematical Sciences, JHU Press, Baltimore, 2013, Chap. 6, pp. 352–355. Section 6.5.4: Cholesky Updating and DOWndating.